Photochemical Electron Transfer in Chromophore–Quencher Complexes of Ru^{II} Based on Tris(1-pyrazolyl)methane

Wayne E. Jones, Jr.,[†] Carlo A. Bignozzi,*[‡] Pingyun Chen,[†] and Thomas J. Meyer*[†]

Chemistry Department, Venable Hall, University of North Carolina, Chapel Hill, North Carolina 27599-3290, and Dipartimento di Chimica, Università di Ferrara, Via L. Borsari N. 46, 44100 Ferrara, Italy

Received September 10, 1992

A series of Ru-based chromophore–quencher complexes have been prepared and characterized. The complexes are based on tris(1-pyrazolyl)methane (tpm), which is a facial, tridentate ligand. Complexes have been prepared containing the electron transfer donor PTZ in bpy-PTZ (bpy-PTZ is 4-methyl-4′-(*N*-phenothiazylmethyl)-2,2′-bipyridine), the electron transfer acceptor MQ^+ (MQ^+ is *N*-methyl-4,4′-bipyridinium cation), and a complex which contains both. Laser flash or steady-state photolysis of $[Ru(tpm)(bpy\text{-}PTZ)(py)]^{2+}$ in CH_3CN at room temperature results in ligand loss photochemistry, no observable emission, and no sign of a long-lived transient. As the temperature was decreased in a 4:1 (v:v) ethanol–methanol solution below 200 K, evidence was obtained by transient absorption spectroscopy for the appearance of the redox-separated state $[Ru^{III}(tpm)(bpy^{\bullet-}\text{-}PTZ^+)(py)]^{2+*}$. Laser flash photolysis of $[Ru^{II}(tpm)(bpy)(MQ^+)]^{3+}$ in CH_3CN gave a weakly emitting excited state ($\Phi_{em} = 3 \times 10^{-4}$; $E_{em} = 765$ nm; $\tau = 300$ ns), which, from its transient absorption difference spectrum, is assigned to the MQ^+-based metal-to-ligand charge transfer (MLCT) excited state $[Ru^{III}(tpm)(bpy)(MQ^{\bullet})]^{3+*}$. Laser flash excitation of $[Ru^{II}(tpm)(bpy\text{-}PTZ)(MQ^+)]^{3+}$ resulted in the appearance of the $MQ^{\bullet}$-based, MLCT state $[Ru^{III}(tpm)(bpy\text{-}PTZ)(MQ^{\bullet})]^{3+*}$ and, to a lesser extent (0.14 ± 0.03), the redox-separated state $[Ru^{II}(tpm)(bpy\text{-}PTZ^+)(MQ^{\bullet})]^{3+}$. This combination of states was reached with an efficiency that was lower by ~2 than the efficiency of formation of $[Ru^{III}(tpm)(bpy)(MQ^{\bullet})]^{3+*}$. The two states are dynamically coupled by intramolecular $PTZ \rightarrow Ru^{III}$ electron transfer. Below 200K in 4:1 (v:v) ethanol–methanol, the excited state properties of the triad are essentially superimposable with those of $[Ru^{II}(tpm)(bpy)(MQ^+)]^{3+}$. The photochemical and photophysical properties of these complexes are discussed in the context of the various states that are accessible and the intramolecular electron transfer processes that occur following laser flash excitation.

Introduction

Considerable progress has been made in learning how to control photoinduced, intramolecular electron and energy transfer within complex molecules.[1] Systematic procedures are appearing for the preparation of chromophore–quencher complexes in which photoexcitation followed by electron transfer leads to the separation and transient storage of oxidative and reductive equivalents within a single molecule. Many of these studies have utilized organic molecules,[2–4] but polypyridyl complexes of Re^{I}, Os^{II}, and Ru^{II} have also proven to be of value and offer special characteristics of their own.[5–7] In these complexes the photochemistry is initiated by metal-to-ligand charge transfer (MLCT) excitation and the excited states can be tuned systematically by varying the ligands.[5–7] The excited states undergo facile electron transfer and the synthetic chemistry is available for attaching electron transfer donors and acceptors. In such assemblies excitation and electron transfer can lead to redox separated states where the oxidative and reductive equivalents occupy sites that are separated spatially.[8]

Much of our own work has been based on complexes of Re^{I} such as $[Re(bpy)(CO)_3(py\text{-}PTZ)]^+$ (bpy is 2,2′-bipyridine) or $[Re^{I}(bpy)(CO)_3(MQ^+)]^{2+}$ in which either a single electron transfer donor (–PTZ, phenothiazinyl) or acceptor (–MQ^+, *N*-methyl-4,4′-bipyridinium ion) are bound through a pyridyl linkage.[9,10] These complexes are free of complications arising from low-lying ligand field (dd) states, there is only a single

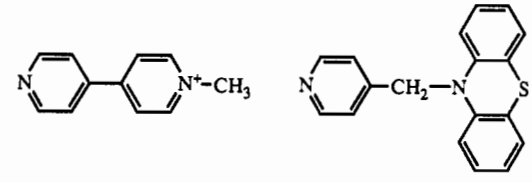

MQ^+ py-PTZ

[†] University of North Carolina.
[‡] Università di Ferrara.

(1) (a) Balzani, V.; Scandola, F. *Supramolecular Photochemistry*; Ellis Horwood: Chichester, U.K., 1990. (b) *Photoinduced Electron Transfer*; Fox, M. A., Chanon, M., Eds.; Elsevier: New York, 1988.
(2) (a) De Schryver, F. C.; Boens, N.; Rut, J. *Adv. Photochem.* **1977**, *10*, 359. (b) Maki, A. H.; Weers, J. G.; Hilinski, E. F.; Milton, S. V.; Rentzepis, P. M. *J. Chem. Phys.* **1984**, *80*, 2288. (c) Closs, G. L.; Piotrowiak, P.; McInnis, J. M.; Fleming, G. R. *J. Am. Chem. Soc.* **1988**, *110*, 2652. (d) Oevering, H.; Verhoeven, J. W.; Paddon-Row, M. N.; Cotsaris, E.; Hush, N. S. *Chem. Phys. Lett.* **1988**, *143*, 488. (e) Zimmerman, H. E.; Weber, A. M. *J. Am. Chem. Soc.* **1989**, *111*, 995, 1007.
(3) (a) Closs, G. L.; Miller, J. R. *Science* **1988**, *240*, 440 and references therein. (b) Johnson, M. D.; Miller, J. R.; Green, N. S.; Closs, G. L. *J. Phys. Chem.* **1989**, *4*, 1173. (c) Heitele, H.; Finckh, P.; Weeren, S.; Pollinger, F.; Michel-Beyerle, M. E. *J. Phys. Chem.* **1989**, *91*, 5173. (d) Gubelmann, M.; Harriman, A.; Lehn, J.; Sessler, J. L. *J. Phys. Chem.* **1990**, *94*, 308 and references therein.
(4) (a) Gaines, L. G.; O'Neil, M. P.; Svec, W. A.; Niemczyk, M. P.; Wasielewski, M. R. *J. Am. Chem. Soc.* **1991**, *113*, 719. (b) Gust, D.; Moore, T. A.; Moore, A. L.; et al. *J. Am. Chem. Soc.* **1991**, *113*, 3638.
(5) (a) Meyer, T. J. *Acc. Chem. Res.* **1989**, *22*, 163. (b) Special issue of *Coord. Chem. Rev.* **1990**, *97*. (c) Scandola, F.; Indelli, M. T.; Chiorboli, C.; Bignozzi, C. A. *Top. Cur. Chem.* **1990**, 158.
(6) (a) Seddon, K. R. *Coord. Chem. Rev.* **1982**, *41*, 79. (b) Ferguson, J.; Herren, F.; Krausz, E. R.; Maeder, M.; Vrbancich, J. *Coord. Chem. Rev.* **1982**, *41*, 159. (c) Meyer, T. J. *Pure Appl. Chem.* **1986**, *58*, 1193.
(7) (a) Lumpkin, R. S.; Kober, E. M.; Worl, L. A.; Murtaza, Z.; Meyer, T. J. *J. Phys. Chem.* **1990**, *94*, 239. (b) Barqawi, K. R.; Llobet, A.; Meyer, T. J. *J. Am. Chem. Soc.* **1988**, *110*, 7751.
(8) (a) Danielson, E.; Elliott, C. M.; Merkert, J. W.; Meyer, T. J. *J. Am. Chem. Soc.* **1987**, *109*, 2519. (b) Mecklenberg, S.; Peek, B.; Erickson, B. W.; Meyer, T. J. *J. Am. Chem. Soc.* **1991**, *113*, 8540. (c) Collin, J.-P.; Guilerez, S.; Sauvage, J.-P.; Barigelletti, F.; Cola De, L.; Flamigni, L.; Balzani, V. *Inorg. Chem.* **1991**, *30*, 4230.

0020-1669/93/1332-1167$04.00/0

M-bpy chromophoric unit, and the preparative chemistry is well developed. Photophysical studies have led to the discovery of new processes and it has been possible to examine such features as the solvent and free energy dependences of back electron transfer to the ground states.[10,11]

There is a continuing need for the design of new families of metal complexes for these studies both to gain insight into the underlying photophysics and to expand the scope of the chemistry. For example, even with their advantages, complexes of Re^{I} have the disadvantage of not absorbing appreciably in the visible and there is a severe compression of absorption features in the near UV which precludes most excitation dependence studies. The requirements for a new family of complexes include the ability to attach ligands containing electron donors or acceptors in separate steps, a visible chromophore, and sufficient photochemical stability to allow electron transfer to occur without decomposition.

In earlier papers we reported on the properties of complexes of Ru^{II} containing derivatives of 2,2′-bipyridine and tris(1-pyrazolyl)methane (tpm).[7b,12] In this manuscript we report an

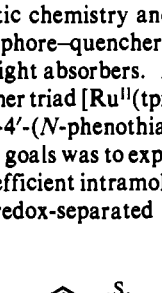

tpm

extension of the synthetic chemistry and photophysical studies to analogs of the chromophore–quencher complexes of Re^{I} which are appreciable visible light absorbers. Among these analogs is the chromophore–quencher triad $[Ru^{II}(tpm)(bpy\text{-}PTZ)(MQ^{+})]^{3+}$ (bpy-PTZ is 4-methyl-4′-(*N*-phenothiazylmethyl)-2,2′-bipyridine). One of our major goals was to explore whether $Ru^{II}\rightarrow bpy$ excitation could lead to efficient intramolecular electron transfer and formation of the redox-separated state, $[Ru^{II}(tpm)(bpy\text{-}PTZ^{+})(MQ^{\bullet})]^{3+}$.

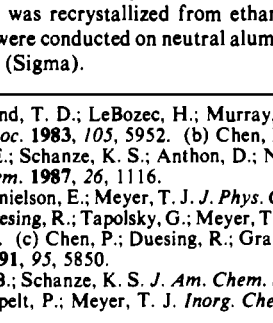

bpy-PTZ

Experimental Section

Materials. All reagents were ACS grade and used without further purification. The compounds 2,2′-bipyridine (bpy), 4,4′-dimethyl-2,2′-bipyridine (dmb) and 4-ethylpyridine (4-Etpy) were purchased from Aldrich. Spectrograde solvents (Burdick and Jackson) were used for the spectroscopic and electrochemical measurements and were used without further purification. Tetra-*n*-butylammonium hexafluorophosphate, $[N(n\text{-}C_4H_9)_4](PF_6)$, was recrystallized from ethanol. The chromatographic separations were conducted on neutral aluminum oxide (Merck) or Sephadex LH-20 (Sigma).

Preparations. Tris(1-pyrazolyl)methane (tpm),[13a] *N*-methyl-4,4′-bipyridinium iodide [MQ]I,[13b] and 4-methyl-4′-(*N*-phenothiazylmethyl)-2,2′-bipyridine (bpy-PTZ),[9,10] were prepared by literature methods. The $[MQ]PF_6$ salt was prepared by metathesis with NH_4PF_6.

The complexes $[Ru(NH_3)_5(MQ^{+})](PF_6)_3$,[13b] $Ru(tpm)Cl_3$,[12] $[Ru(tpm)(dmb)Cl]Cl$,[12] $[Ru(tpm)(dmb)(H_2O)](PF_6)_2$,[12] $[Ru(tpm)(bpy)(4\text{-}Etpy)](PF_6)_2$,[7b] $[Ru(tpm)(dmb)(py)](PF_6)_2$,[12] $K_2[Ru(CN)_5(MQ^{+})]$,[14] $[Re(CO)_3(MQ^{+})_2Cl](PF_6)_2$,[15] and $[Re(bpy\text{-}PTZ)(CO)_3(4\text{-}Etpy)](PF_6)$[9,10] were prepared or were available from previous studies.

$[Ru(tpm)(bpy\text{-}PTZ)Cl]Cl\cdot 3H_2O$. A 0.32 g amount of $Ru(tpm)Cl_3$ (0.76 mmol), 0.29 g of bpy-PTZ (0.76 mmol) and 0.3 g of LiCl were dissolved in 80 mL of an ethanol/water (3:1) solution and heated at reflux under Ar for 15 min. Twelve drops of triethylamine were added and the mixture was heated at reflux for 5 h. Thin-layer chromatography on alumina plates with methanol showed the presence of three components: a blue, unidentified species (R_f = 0.1–0.2), the desired yellow-orange product (R_f = 0.4), and unreacted ligand (R_f = 0.65). The brown solution was filtered hot and taken to dryness by roto-evaporation. The solid was dissolved in methanol and loaded onto a 4 × 30 cm neutral alumina column. After complete elution of the unreacted ligand, the yellow-orange fraction was collected and evaporated to dryness. The complex was recrystallized from methanol, giving dark red crystals. Yield: 48%. Anal. Calc for $C_{34}H_{37}Cl_2N_9O_3SRu$: C, 49.57; H, 4.53; N, 15.30. Found: C, 48.71; H, 4.52; N, 14.96.

$[Ru(tpm)(bpy\text{-}PTZ)(H_2O)](PF_6)_2\cdot 2H_2O$. A 0.3 g quantity of $[Ru(tpm)(bpy\text{-}PTZ)Cl]Cl\cdot 3H_2O$ (0.36 mmol) was dissolved in 80 mL of a methanol/water (1:1) solution, 0.18 g of $AgPF_6$ (0.72 mmol) were added and the solution was heated at reflux for 2 h under Ar. After cooling, AgCl was filtered off and the volume of the solution reduced to 40 mL. A few drops of a saturated solution of NH_4PF_6 were added and the salt that precipitated, collected by filtration, washed with cold water and vacuum dried over $CaCl_2$. Yield: 90%. Anal. Calc for $C_{34}H_{35}O_3N_9SP_2F_{12}Ru$: C, 39.24; H, 3.39; N, 12.11. Found: C, 38.72; H, 3.40; N, 11.82.

$[Ru(tpm)(bpy\text{-}PTZ)(py)](PF_6)_2$. A 0.15 g amount of $[Ru(tpm)(bpy\text{-}PTZ)(H_2O)](PF_6)_2$ and 1 ml of pyridine were heated at reflux in 20 mL of a 0.1 M NH_4PF_6 aqueous solution for 4 h. The solution was cooled to room temperature and 20 mL of water were added with stirring. The precipitate was filtered, washed with water and then ether and vacuum dried. The solid was dissolved in CH_3CN and chromatographed on a 2 × 25 cm Sephadex LH 20 column with CH_3CN as eluent. Three components were resolved. The main fraction was collected, concentrated to a few mL and loaded onto a 2 × 15 cm neutral alumina column in CH_3CN 5% in CH_3OH. A small amount of a yellow component was irreversibly retained by the column. The eluted fraction was evaporated to dryness and the solid recrystallized twice from methanol/ether. Yield: 56%. Anal. Calc for $C_{39}N_{10}H_{36}SP_2F_{12}Ru$: C, 43.87; H, 3.40; N, 13.12. Found: C, 42.96; H, 3.28; N, 12.71.

$[Ru(tpm)(bpy\text{-}PTZ)(MQ^{+})](PF_6)_3$. A 0.27 g amount of $[Ru(tpm)(bpy\text{-}PTZ)(H_2O)](PF_6)_2\cdot 2H_2O$ (0.26 mmol) in 70 mL of a 0.05 M NH_4PF_6 aqueous solution was added to 0.66 g of $[MQ]PF_6$ (2.09 mmol) in 30 mL of acetone and heated at reflux for 60 h. The solution was evaporated to 70 mL, cooled and the orange product precipitated by dropwise addition to an aqueous solution saturated in NH_4PF_6. The solid was air dried, dissolved in acetone and loaded onto a 3 × 15 cm neutral alumina column. Elution was first performed with acetone to recover the unreacted $[MQ]PF_6$ and then with warm methanol to collect the orange fraction. This fraction was evaporated to dryness and the solid recrystallized twice from acetone/ether. Yield: 80%. Anal. Calc for $C_{45}N_{11}H_{42}SP_3F_{18}Ru$: C, 41.42; H, 3.24; N, 11.81. Found: C, 41.29; H, 3.10; N, 12.04.

$[Ru(tpm)(bpy)(MQ^{+})](PF_6)_3$. A 0.20 g amount of $[Ru(tpm)(bpy)(H_2O)](PF_6)_2$,[12] (0.09 mmol) and 0.057 g of $[MQ]PF_6$, (0.18 mmol) dissolved in a 25 mL 0.1 M NH_4PF_6 in water were heated at reflux for 6 h. Orange crystals were observed to form gradually. The suspension was cooled to room temperature and filtered. The orange crystals were washed with water and dried under vacuum. Yield: 70%. Anal. Calc for $C_{33}N_{10}H_{34}P_3F_{18}Ru$: C, 34.55; H, 2.71; N, 13.0. Found: C, 34.37; H, 2.74; N, 12.49.

Measurements. Electrochemical data were obtained by cyclic voltammetry with a PAR model 173 potentiostat and a triangular waveform

(9) (a) Westmoreland, T. D.; LeBozec, H.; Murray, R. W.; Meyer, T. J. *J. Am. Chem. Soc.* **1983**, *105*, 5952. (b) Chen, P.; Westmoreland, T. D.; Danielson, E.; Schanze, K. S.; Anthon, D.; Neveux, P. E.; Meyer, T. *J. Inorg. Chem.* **1987**, *26*, 1116.
(10) (a) Chen, P.; Danielson, E.; Meyer, T. J. *J. Phys. Chem.* **1988**, *92*, 3708. (b) Chen, P.; Duesing, R.; Tapolsky, G.; Meyer, T. J. *J. Am. Chem. Soc.* **1989**, *111*, 7448. (c) Chen, P.; Duesing, R.; Graff, D.; Meyer, T. J. *J. Phys. Chem.* **1991**, *95*, 5850.
(11) MacQueen, D. B.; Schanze, K. S. *J. Am. Chem. Soc.* **1991**, *133*, 7470.
(12) Llobet, A.; Doppelt, P.; Meyer, T. J. *Inorg. Chem.* **1988**, *27*, 514.
(13) (a) Huckel, W.; Bretschneider, H. *Ber. Chem.* **1937**, *9*, 2024. (b) Curtis, J. F.; Sullivan, B. P.; Meyer, T. J. *Inorg. Chem.* **1983**, *22*, 224.
(14) Bignozzi, C. A.; Timpson, C. J.; Kober, E. M.; Sullivan, B. P.; Meyer, T. J. Manuscript in preparation.
(15) Chen, P.; Jones, W. E.; Meyer, T. J. Manuscript in preparation.

generator with the output plotted on a Hewlett-Packard 7015 XY recorder. The experiments were performed in argon deaerated CH_3CN solutions, with Pt-bead working, Pt-wire auxiliary and saturated sodium calomel (SSCE) reference electrodes in a single compartment cell. Values of $E_{1/2}$ were calculated by averaging the oxidative $E_{p,a}$ and reductive $E_{p,c}$ peak potentials in 0.1 M $[N(n\text{-}C_4H_9)_4](PF_6)$ and were not corrected for junction potentials. Controlled-potential electrolyses were performed with an Amel 568 programmable function generator and an Amel 552 potentiostat.

Spectra of the electrochemically reduced or oxidized species were obtained with an OTTLE (optically transparent thin-layer electrode) made of a platinum (90%)–rhodium (10%) grid (Johnson Mathey) placed between the windows of a 2 mm spectrophotometric cell directly mounted in a Perkin-Elmer 323 spectrophotometer or Hewlett-Packard Model 9451A UV/vis-diode array spectrophotometer. The counter-electrode was a Pt wire separated from the cathodic compartment by a frit; a Ag wire was used as a reference electrode. The measured difference between the redox potentials of the Ag and SCE reference electrodes was –0.15 V. All of the spectroelectrochemical experiments were carried out in acetonitrile (Carlo Erba or Burdick and Jackson) which contains 0.1 M $[N(n\text{-}C_4H_9)_4](PF_6)$ as the supporting electrolyte. Before reduction, the solutions were purged with argon for 15 min directly in the spectrophotometric cell. In the controlled potential electrolysis experiments (CPE), the final electronic spectra of the reduced or oxidized species were taken to have been reached when there was no further change in the absorption spectra and when minimal current was being passed.

UV–vis spectra were recorded on Cary 17 or Hewlett-Packard Model 9451A UV/vis-diode array spectrophotometers. Infrared spectra were recorded in KBr pellets with a Nicolet 20DX FTIR spectrophotometer or with a IFS88 Bruker FTIR spectrophotometer.

Steady state emission measurements were obtained on a SPEX Fluorolog-212A spectrofluorimeter with a Hamamatsu R636 red-sensitive photomultiplier tube by using 420 nm, monochromatic light from a 450 W xenon lamp as the excitation source. Emission quantum yields were determined at room temperature in dilute (o.d. ~ 0.1) acetonitrile solutions by relative actinometry by using eq 1.[16] In this equation Φ is the emission

$$\Phi_2 = \Phi_1(I_2/I_1)(n_2/n_1)^2(A_1/A_2) \quad (1)$$

quantum yield of either the known or unknown (subscript 1 or 2 respectively), I is the integrated sum of the emission intensity, n is the refractive index of the solvent, and A is the absorbance in a 1 cm cuvette cell. The known quantum yield used in this study was $\Phi_{em} = 0.062$ for $[Ru(bpy)_3]^{2+}$ in acetonitrile.[17] Time-resolved emission measurements were made by using a PRA LN1000/LN102 nitrogen laser/dye laser combination for excitation (λ = 457 nm, Coumarin 460). Emission was monitored at right angles by using a PRA B204-3 monochromator and a cooled, 10-stage, Hamamatsu R928 photomultiplier. The output from the PMT was terminated through 50 Ω to a LeCroy 6880 GHz digitizer with a LeCroy 350 MHz amplifier, or a LeCroy 9400 125 MHz digitizing oscilloscope. Either digitizer was interfaced to a personal computer, with software of our own design, for data analysis and workup. Samples were prepared at ~1×10^{-5} M in acetonitrile solutions which were deoxygenated by either bubbling with Ar (15 min) or by freeze–pump–thaw degassing through a minimum of 4 cycles (10^{-6} Torr).

Transient absorption measurements were conducted with a system partially described elsewhere.[18] The system incorporates a Quanta Ray DCR-2A Nd:YAG laser with the third harmonic of the fundamental separated and coupled to a Quanta Ray PDL-2 dye laser. The excitation beam was either perpendicular to, or co-axial (using appropriate dichroic optics from CVI East) with an Applied Photophysics laser kinetic spectrometer with a 250 W pulsed Xenon lamp, f3.4 monochromator, and a Hamamatsu R446 photomultiplier tube. The output of the photomultiplier was coupled to either LeCroy 9400 or 6880 digitizing oscilloscopes which had been interfaced to a personal computer. Electronic synchronization and control of the experiment was achieved through electronics of our own design.[18] In these experiments the samples were prepared as above for the time-resolved emission measurements at a concentration of (1–4) $\times 10^{-5}$ M. Temperature control for the temperature dependent emission and absorption measurements was achieved with an Oxford DN 1704 cryostat with an Oxford 3120 temperature controller. The temperature was independently measured using an external thermocouple to be ±3 K. The laser excitation energy was determined to be 1–4 mJ/pulse at 1 Hz by using a Molectron J-9 Joulemeter and a spot diameter of ~0.2 mm for the dye laser.

Kinetic analysis of the transient absorption and emission data was achieved by using software developed locally[18] based on a modified Levenberg–Marquardt non-linear least-squares, iterative fitting procedure.[19] The best fit to the data was judged by following the sum of the squared errors and visually monitoring the residuals. The absorbance data were analyzed as absorbance change (ΔA) vs time traces where the absorbance change was related to the initial intensity (I_0) and the change in intensity (ΔI) by the equation $\Delta A = \log[I_0/(I_0 + \Delta I)]$. The quantity I_0 was taken as the voltage corresponding to the current, produced by the background monitoring light incident upon the photomultiplier, terminated into 50 Ω, and ΔI was the change in that voltage following the laser flash.

Results

Infrared Spectra. IR spectra were recorded in the 4000–400-cm^{-1} region. The spectra of $[Ru(tpm)(bpy\text{-}PTZ)(MQ^+)](PF_6)_3$ and $[Ru(tpm)(bpy)(MQ^+)](PF_6)_3$ were superimposable with the sum of the spectra of the appropriate components $Ru(tpm)(Cl)_3$, $[Ru(tpm)(bpy\text{-}PTZ)Cl](PF_6)$ or $[Ru(tpm)(dmb)Cl](PF_6)$ and $[Ru(NH_3)_5(MQ^+)](PF_6)_3$. Bands for the framework stretching modes for coordinated tpm, dmb, and MQ^+ appear in the 1700–1000-cm^{-1} range. By comparison with spectra of $[Ru(bpy)_3](PF_6)_2$, $[Ru(dmb)_3](PF_6)_2$, and $[Re(bpy\text{-}PTZ)(CO)_3(4\text{-}Etpy)](PF_6)$, intense bands observed for $[Ru(tpm)(bpy\text{-}PTZ)(MQ^+)](PF_6)_3$ and $[Ru(tpm)(bpy)(MQ^+)](PF_6)_3$ at 1620, 1466, 1447, 1412, and 1225 cm^{-1} can be assigned to stretching modes of the bipyridine ligand. The bands at 1412 and 1225 cm^{-1} are, in part, overlapped with bands at 1406 and 1227 cm^{-1} for the tpm ligand. Additional, intense tpm bands are observed at 1272, 1243, 1093 and 1060 cm^{-1}. Bands at 1643, 1194 cm^{-1} and 1649, 1197 cm^{-1}, respectively, in the spectra of $[Ru(tpm)(bpy\text{-}PTZ)(MQ^+)](PF_6)_3$ and $[Ru(tpm)(bpy)(MQ^+)](PF_6)_3$, arise from ring stretching modes of the coordinated MQ^+ ligand by comparison with the spectra of $[Ru(NH_3)_5(MQ^+)](PF_6)_3$[13b] and $[Ru(CN)_5(MQ^+)]^{2-}$.[14]

Electrochemistry. Voltammetric half-wave potentials ($E_{1/2}$) were measured by cyclic voltammetry in CH_3CN solution. The results are reported in Table I. For purposes of comparison, reduction potentials for model complexes containing the $-MQ^+$ ligand and potentials for the $MQ^{+/0}$ and $PQ^{2+/+}$, and $PQ^{+/0}$ couples (PQ^{2+} is *N*,*N*-dimethyl-4,4′-bipyridinium dication)[20] and the potential for the bpy-$PTZ^{+/0}$ couple are also reported. In the oxidative range explored (0 to +1.8 V), peak currents were comparable to those for reduction waves in the cathodic scans from 0 to –1.8 V. Although peak to peak separations, ΔE_p, range from 60 to 75 mV, the electrode reactions are essentially electrochemically reversible. This is shown by the invariance of anodic and cathodic peak potentials to scan rates in the range 100–400 mV/s and by the ratio of the anodic and cathodic peak currents of near one.

Electronic Spectra. UV–vis spectra were recorded in CH_3CN. Absorption band energies and assignments are reported in Table II. The major bands for $[Ru(tpm)(dmb)X]^{n+}$ (n = 1, X = Cl; n = 2, X = H_2O, py) have been assigned previously.[7b] The near UV–visible region is dominated by $d\pi(Ru) \rightarrow \pi_1^*(dmb)$ MLCT bands and overlapping $d\pi(Ru) \rightarrow \pi^*(tpm)$ and $d\pi(Ru) \rightarrow \pi_2^*(dmb)$ bands (310–390 nm). The bands at 290 nm result from overlapping $\pi \rightarrow \pi_1^*$ transitions centered on the dmb and tpm ligands and $\pi \rightarrow \pi_2^*(dmb)$ appear ~5500 cm^{-1} higher in energy.

(16) (a) Parker, C. A.; Rees, W. T. *Analyst (London)* **1960**, *85*, 587. (b) Allen, G. H.; White, R. P.; Rillema, D. P.; Meyer, T. J. *J. Am. Chem. Soc.* **1984**, *106*, 2613.
(17) Caspar, J. V.; Meyer, T. J. *J. Am. Chem. Soc.* **1983**, *105*, 5583.
(18) Danielson, E. Ph.D. Dissertation, University of North Carolina, in preparation.
(19) (a) Seber, G. A.; Wild, C. J. *Non-Linear Regression*; Wiley: New York, 1987. (b) Levenberg, K. *Q. Appl. Math.* **1944**, *2*, 164. (c) Marquardt, D. W. *J. Soc. Ind. Appl. Math.* **1963**, *11*, 431.
(20) Mackay, R. A.; Landolph, J. R.; Poziomek, E. J. *J. Am. Chem. Soc.* **1971**, *93*, 5026.

Table I. Redox Potentials in 0.1 M $[N(n\text{-}C_4H_9)_4](PF_6)$–$CH_3CN$ solution at 298 K ($E_{1/2}$, V vs SSCE)

complex or ligand	$Ru^{III/II}$	$PTZ^{+/0}$	$MQ^{+/0}$ or $PQ^{2+/+}$	$bpy^{0/-}$	$MQ^{0/-}$ or $PQ^{+/0}$
$[Ru(tpm)(dmb)Cl]^{+}$ [a,b]	+0.70			−1.61	
$[Ru(tpm)(dmb)(H_2O)]^{2+}$	+1.04			−1.42	
$[Ru(tpm)(bpy)(4\text{-Etpy})]^{2+}$	+1.15			−1.38	
$[Ru(tpm)(bpy)(MQ^{+})]^{3+}$	+1.25		−0.77	−1.34	−1.53
$[Ru(tpm)(dmb)(py)]^{2+}$ [b]	+1.15			−1.39	
$[Ru(tpm)(bpy\text{-}PTZ)Cl]^{+}$	+0.65	+0.81		−1.60	
$[Ru(tpm)(bpy\text{-}PTZ)(H_2O)]^{2+}$	+1.00	+0.81		−1.45	
$[Ru(tpm)(bpy\text{-}PTZ)(py)]^{2+}$	+1.14	+0.79		−1.42	
$[Ru(tpm)(bpy\text{-}PTZ)(MQ^{+})]^{3+}$	+1.20	+0.80	−0.80	−1.37	−1.57
$[Ru(NH_3)_5(MQ^{+})]^{3+}$	+0.39		−0.92		−1.55
$[Re(MQ^{+})_2(CO)_3Cl]^{2+}$	+1.48		−0.75		−1.32, −1.44
bpy-PTZ		+0.80			
MQ^{+}			−0.98		−1.71
PQ^{2+} [c]			−0.46		+0.70

[a] All complexes were PF_6^- salts except for $[Ru(tpm)(bpy)Cl]Cl$. [b] From ref 12. [c] From ref 13b.

Table II. UV–Visible Absorption Maxima in CH_3CN

complex	λ_{max}, nm (ϵ, M^{-1} cm^{-1})	assgnt	complex	λ_{max}, nm (ϵ, M^{-1} cm^{-1})	assgnt
$[Ru(tpm)(dmb)Cl]Cl$[a]	475	$d\pi\rightarrow\pi_1^*$ (bpy)	$[Ru(tpm)(bpy\text{-}PTZ)(H_2O)](PF_6)_2$	470 (3050)	$d\pi\rightarrow\pi_1^*$ (bpy)
	440	$d\pi\rightarrow\pi_1^*$ (bpy)		415 (3700)	$d\pi\rightarrow\pi_1^*$ (bpy)
	335	$d\pi\rightarrow\pi_2^*$ (bpy)		330 (13 000)	$d\pi\rightarrow\pi_2^*$ (bpy)
		$d\pi\rightarrow\pi^*$ (tpm)			$d\pi\rightarrow\pi^*$ (tpm)
	289	$\pi\rightarrow\pi_1^*$ (bpy)		290 (27 500)	$\pi\rightarrow\pi_1^*$ (bpy)
	243, 255	$\pi\rightarrow\pi^*$		254 (34 600)	$\pi\rightarrow\pi^*$
$[Ru(tpm)(dmb)(CH_3CN)](PF_6)_2$	475	$d\pi\rightarrow\pi_1^*$ (bpy)	$[Ru^{II}(tpm)(bpy\text{-}PTZ)(py)](PF_6)_2$	470 (2550)	$d\pi\rightarrow\pi_1^*$ (bpy)
	425	$d\pi\rightarrow\pi_1^*$ (bpy)		415 (4550)	$d\pi\rightarrow\pi_1^*$ (bpy)
	328	$d\pi\rightarrow\pi_2^*$ (bpy)		330 (14 000)	$d\pi\rightarrow\pi_2^*$ (bpy)
		$d\pi\rightarrow\pi^*$ (tpm)			$d\pi\rightarrow\pi^*$ (tpm)
	291	$\pi\rightarrow\pi_1^*$ (bpy)		300 (sh, 30 000)	$\pi\rightarrow\pi_1^*$ (bpy)
	243, 255	$\pi\rightarrow\pi^*$		254 (45 500), 289 (34 000)	$\pi\rightarrow\pi^*$
$[Ru(tpm)(bpy)(4\text{-Etpy})](PF_6)_2$	470 (2050)	$d\pi\rightarrow\pi_1^*$ (bpy)			
	420 (4540)	$d\pi\rightarrow\pi_1^*$ (bpy)	$[Ru(tpm)(bpy\text{-}PTZ)(MQ^{+})](PF_6)_3$	470 (10 000)	$d\pi\rightarrow\pi_1^*$ (bpy)
	340 (15 000)	$d\pi\rightarrow\pi_2^*$ (bpy)			$d\pi\rightarrow\pi_1^*$ (MQ^{+})
		$d\pi\rightarrow\pi^*$ (tpm)		420 (8200)	$d\pi\rightarrow\pi_1^*$ (bpy)
	289 (28 630)	$\pi\rightarrow\pi_1^*$ (bpy)		330 (sh, 12 200)	$d\pi\rightarrow\pi_2^*$ (bpy)
					$d\pi\rightarrow\pi^*$ (tpm)
	244 (15 450), 254 (11 360)	$\pi\rightarrow\pi^*$		300 (sh, 30 400)	$\pi\rightarrow\pi_1^*$ (bpy)
				254 (55 000), 287 (37 100)	$\pi\rightarrow\pi^*$
$[Ru^{II}(tpm)(bpy)(MQ^{+})](PF_6)_2$	465 (13 200)	$d\pi\rightarrow\pi^*$ (MQ^{+})			
		$d\pi\rightarrow\pi_1^*$ (bpy)	$[MQ^{+}](PF_6)$	261 (18 300)	$\pi\rightarrow\pi^*$ (MQ^{+})
	420 (10 000)	$d\pi\rightarrow\pi_1^*$ (bpy)	bpy-PTZ	282 (15 700)	$\pi\rightarrow\pi_1^*$ (bpy)
	340 (sh, 7700)	$d\pi\rightarrow\pi_2^*$ (bpy)		252 (39 400)	$\pi\rightarrow\pi^*$
		$d\pi\rightarrow\pi^*$ (tpm)	$[Ru^{II}(NH_3)_5(MQ^{+})](PF_6)_3$	580 (16 000)	$d\pi\rightarrow\pi^*$ (MQ^{+})
	300 (sh, 25 000)	$\pi\rightarrow\pi_1^*$ (bpy)	$[Re(CO)_3(MQ^{+})_2Cl](PF_6)_2$	350 (11 000)	$d\pi\rightarrow\pi^*$ (MQ^{+})
	256 (32 000), 286 (35 200)	$\pi\rightarrow\pi^*$	$MQ^{\bullet}$ [b]	534 (11 200)	$\pi\rightarrow\pi^*$ ($MQ^{\bullet}$)
				370 (33 400)	$\pi\rightarrow\pi^*$ ($MQ^{\bullet}$)
$[Ru(tpm)(dmb)(py)](PF_6)_2$	470 (2050)	$d\pi\rightarrow\pi_1^*$ (bpy)	$[Ru^{II}(NH_3)_5(MQ^{\bullet})](PF_6)_2$[b]	670 (5600)	$\pi\rightarrow\pi^*$ ($MQ^{\bullet}$)
	420 (4540)	$d\pi\rightarrow\pi_1^*$ (bpy)		526 (35 000)	$d\pi\rightarrow\pi^*$ ($MQ^{\bullet}$)
	340 (15 000)	$d\pi\rightarrow\pi_2^*$ (bpy)		360 (19 500)	$\pi\rightarrow\pi^*$ ($MQ^{\bullet}$)
		$d\pi\rightarrow\pi^*$ (tpm)	$[Re^{I}(CO)_3(MQ^{\bullet})_2Cl]$[b]	595 (23 500)	$\pi\rightarrow\pi^*$ ($MQ^{\bullet}$)
	289 (28 630)	$\pi\rightarrow\pi_1^*$ (bpy)		410 (39 500)	$d\pi\rightarrow\pi^*$ ($MQ^{\bullet}$)
	244 (15 450), 254 (11 360)	$\pi\rightarrow\pi^*$		304 (15 000)	$\pi\rightarrow\pi^*$ ($MQ^{\bullet}$)
			$[Ru^{II}(tpm)(bpy)(MQ^{\bullet})](PF_6)_2$[b]	595 (11 500)	$\pi\rightarrow\pi^*$ ($MQ^{\bullet}$)
$[Ru(tpm)(bpy\text{-}PTZ)(Cl)](PF_6)$	500 (4000)	$d\pi\rightarrow\pi_1^*$ (bpy)		480 (29 800)	$d\pi\rightarrow\pi^*$ ($MQ^{\bullet}$, bpy)
	470 (4300)	$d\pi\rightarrow\pi_1^*$ (bpy)		358 (21 000)	$\pi\rightarrow\pi^*$ ($MQ^{\bullet}$)
	330 (9500)	$d\pi\rightarrow\pi_2^*$ (bpy)			$d\pi\rightarrow\pi_2^*$ (bpy)
		$d\pi\rightarrow\pi^*$ (tpm)	$[Ru^{II}(tpm)(bpy\text{-}PTZ)(MQ^{\bullet})]$[b]	595 (8400)	$\pi\rightarrow\pi^*$ ($MQ^{\bullet}$)
	296 (28 200)	$\pi\rightarrow\pi_1^*$ (bpy)		482 (23 000)	$d\pi\rightarrow\pi^*$ ($MQ^{\bullet}$, bpy)
	254 (38 600)	$\pi\rightarrow\pi^*$		358 (18 300)	$\pi\rightarrow\pi^*$ ($MQ^{\bullet}$)
					$d\pi\rightarrow\pi_2^*$ (bpy)

[a] The spectrum of the chloride salt was obtained in H_2O. [b] Obtained by CPE; see text.

The spectra of complexes containing bpy-PTZ were similar except for appearance of $\pi\rightarrow\pi^*$ (PTZ) bands in the UV. Visible absorption bands for $[Ru^{II}(tpm)(bpy)(MQ^{+})]^{3+}$ and $[Ru^{II}(tpm)(bpy\text{-}PTZ)(MQ^{+})]^{3+}$ arise from overlapping $d\pi(Ru)\rightarrow\pi^*(bpy)$ and $d\pi(Ru)\rightarrow\pi^*(MQ^{+})$ transitions. In Figures 1A and 1B are shown the spectra of $[Ru^{II}(tpm)(bpy)(MQ^{+})]^{3+}$ (compared to $[Ru(tpm)(bpy)(4\text{-Etpy})]^{2+}$) and of $[Ru^{II}(tpm)(bpy\text{-}PTZ)(MQ^{+})]^{3+}$ (compared to $[Ru(tpm)(bpy\text{-}PTZ)(py)]^{2+}$). The difference spectra between each pair are shown as insets. In the difference spectra positive absorption features appear at ~260 and 470 nm and a negative feature at 350 nm. The negative feature arises from $d\pi(Ru)\rightarrow\pi^*$(4-Etpy,py) in $[Ru(tpm)(bpy)(4\text{-Etpy})]^{2+}$ and $[Ru(tpm)(bpy\text{-}PTZ)(py)]^{2+}$, and the positive features from $\pi\rightarrow\pi^*(MQ^{+})$ and $d\pi(Ru)\rightarrow\pi^*(MQ^{+})$ bands.

Spectroelectrochemistry. In Figure 2 are shown visible absorption spectra for $[Ru^{II}(tpm)(bpy\text{-}PTZ)(MQ^{+})]^{3+}$ and its one-electron oxidized form obtained by controlled potential electrolysis (CPE) at +1.0 V vs Ag (+0.85 V vs SCE). The spectrum of the oxidized complex is approximately the sum of the visible spectra

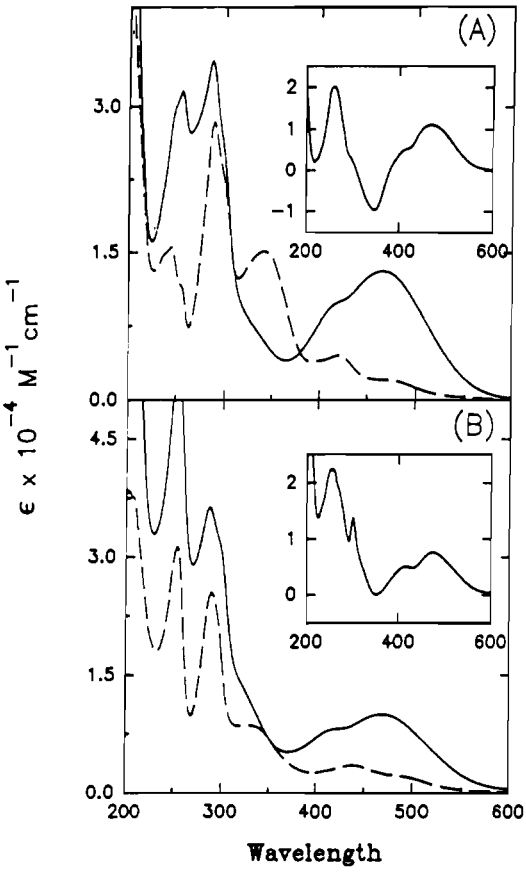

Figure 1. Absorption spectra of (A) $[Ru(tpm)(bpy)(4\text{-}Etpy)]^{2+}$ (- - -), $[Ru^{II}(tpm)(bpy)(MQ^+)]^{3+}$ (—) and (B) $[Ru(tpm)(bpy\text{-}PTZ)(py)]^{2+}$ (- - -) and $[Ru^{II}(tpm)(bpy\text{-}PTZ)(MQ^+)]^{3+}$ (—) at room temperature in acetonitrile. The difference spectra between the respective pairs are shown as inserts.

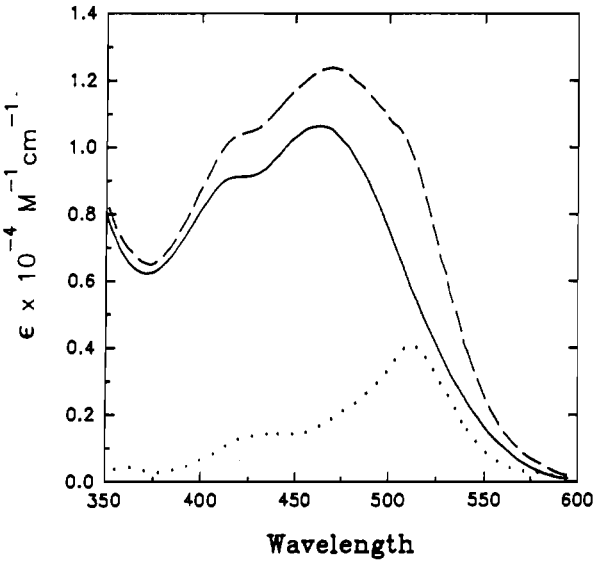

Figure 2. Absorption spectrum of $[Ru^{II}(tpm)(bpy\text{-}PTZ)(MQ^+)]^{3+}$ (—) and the one electron oxidation product $[Ru^{II}(tpm)(bpy\text{-}PTZ^+)(MQ^+)]^{4+}$ (- - -) in acetonitrile. The difference spectrum between the two is also shown (···).

of the 3+ ion and PTZ^+ radical cation, as shown by the difference spectrum. The band that appears at 510 nm in the difference spectrum also appears for bpy-PTZ^+ generated by controlled potential electrolysis of uncoordinated bpy-PTZ at +1.20 V vs Ag (+1.05 V vs SCE). The one-electron oxidized forms of the complex and of bpy-PTZ were stable on the time scale of the CPE experiments (15–20 min). The initial spectra were recovered

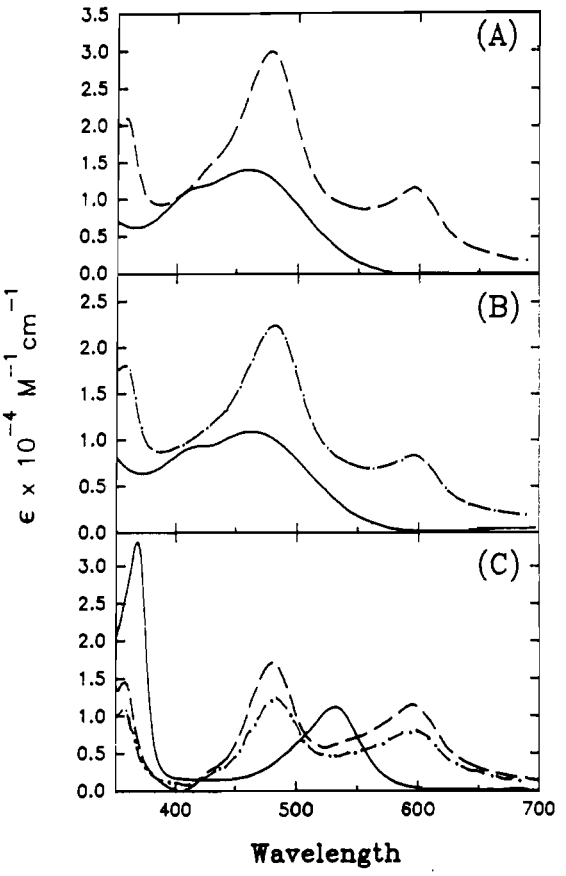

Figure 3. Spectroelectrochemistry in CH_3CN, 0.1 M in $[N(n\text{-}C_4H_9)_4](PF_6)$ of (A) $[Ru^{II}(tpm)(bpy)(MQ^+)]^{3+}$ (—) and its one-electron reduced form $[Ru^{II}(tpm)(bpy)(MQ^{\bullet})]^{2+}$ (- - -), (B) $[Ru^{II}(tpm)(bpy\text{-}PTZ)(MQ^+)]^{3+}$ (—) and its one-electron reduced form $[Ru^{II}(tpm)(bpy\text{-}PTZ)(MQ^{\bullet})]^{2+}$ (- - -), (C) the one-electron reduced form of MQ^+ as PF_6 salt (—) compared to the spectra of the reduced complexes in A (- - -) and B (- - -).

nearly quantitatively upon reduction. Oxidations performed by using Br_2 in acetonitrile gave comparable results.

The one-electron-reduced forms of MQ^+, $[Ru^{II}(tpm)(bpy\text{-}PTZ)(MQ^+)]^{3+}$, $[Ru^{II}(tpm)(bpy)(MQ^+)]^{3+}$, $[Ru^{II}(NH_3)_5(MQ^+)]^{3+}$, and $[Re^{I}(MQ^+)_2(CO)_3(Cl)]^{2+}$ were obtained by electrolysis at –1.1 V vs Ag for MQ^+, at –0.85 V for the tpm complexes, at –1.2 V for the pentaammine complex, and at –1.0 V for the Re complex. For the Re complex this leads to reduction of both of the MQ^+ ligands.

The electronic spectra of $[Ru^{II}(tpm)(bpy)(MQ^+)]^{3+}$ and $[Ru^{II}(tpm)(bpy\text{-}PTZ)(MQ^+)]^{3+}$ are shown in Figure 3A,B, respectively, along with their respective, one-electron reduced forms obtained by CPE. Upon reduction, the visible absorptivity increases noticeably for each with bands appearing at 358, 480 and 595 nm, Figure 3.

Photophysical Properties. Emission characteristics in acetonitrile are summarized in Table III. The emission energy and bandshape for $[Ru(tpm)(bpy)(4\text{-}Etpy)]^{2+}$ are typical of those found for other tpm complexes.[7b] The emission is short-lived with $\tau < 10$ ns and steady state photolysis in acetonitrile led to photodecomposition as evidenced by changes in the MLCT absorption spectra. The steady state emission spectrum in 4:1 ethanol:methanol at 77 K, where the complex is photochemically stable, is shown in Figure 4A.

For $[Ru^{II}(tpm)(bpy)(MQ^+)]^{3+}$ in CH_3CN compared to $[Ru(tpm)(bpy)(4\text{-}Etpy)]^{2+}$ (Table III) there was a decrease in emission quantum yield by a factor of 4, a red shift in the emission maximum to 795 nm, and a 100-fold *increase* in lifetime. Its transient absorption difference spectrum at room temperature is shown in Figure 5A. Positive absorption features appear at 370

Table III. Lifetime and Emission Properties

	CH_3CN, 298 K			4:1 ETOH/MeOH, 77 K	
complex	$\lambda_{max,em}$ (nm)[a] (±2 nm)	τ (ns)[a] (±3%)	Φ_{em}[a] (±5%)	$\lambda_{max,em}$ (nm)[b] (±2 nm)	τ (μs)[b] (±3%)
$[Ru^{II}(tpm)(bpy)(4\text{-}Etpy)](PF_6)_2$	668	<10	1.3×10^{-3}	598	3.70
$[Ru^{II}(tpm)(bpy)(MQ^+)](PF_6)_3$	795	300	3×10^{-4}	596	3.6[c]
$[Ru^{II}(tpm)(bpy\text{-}PTZ)(py)](PF_6)_2$	664	<10	4×10^{-4}	586	4.37
$[Ru^{II}(tpm)(bpy\text{-}PTZ)(MQ^+)](PF_6)_3$	*d*	769 (0.55), 62 (0.45)[e] 847 (0.58), 77 (0.42)[f]		588	4.4[c]

[a] In acetonitrile at 298 K. [b] In 4:1 (v:v) ethanol:methanol at 77 K, the emission maximum reported is the energy of the first vibronic progression. [c] The decay was non-exponential. The lifetime cited is for the dominant component (>90%) in a biexponential fit to eq 2, see text. [d] None observed. [e] These values were derived from bi-exponential fits to transient absorption vs time profiles monitored at 370 nm following 420 nm excitation. The relative weighting factors for the two components are shown in parentheses. [f] Same as *e* monitored at 640 nm.

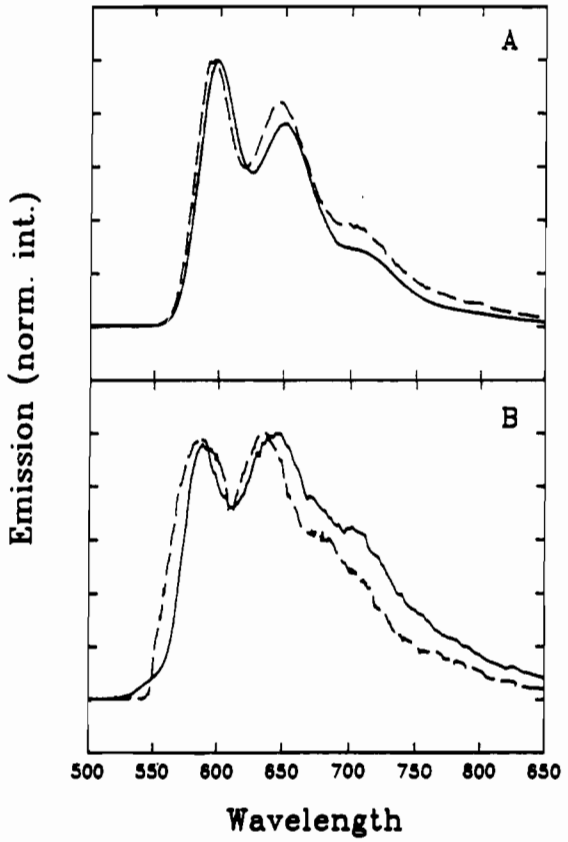

Figure 4. Emission spectra following excitation at 457 nm for (A) $[Ru(tpm)(bpy)(4\text{-}Etpy)]^{2+}$ (- - -) and $[Ru^{II}(tpm)(bpy)(MQ^+)]^{3+}$ (—) and (B) $[Ru(tpm)(bpy\text{-}PTZ)(py)]^{2+}$ (- - -) and $[Ru^{II}(tpm)(bpy\text{-}PTZ)(MQ^+)]^{3+}$ (—) in 4:1 EtOH:MeOH at 77 K.

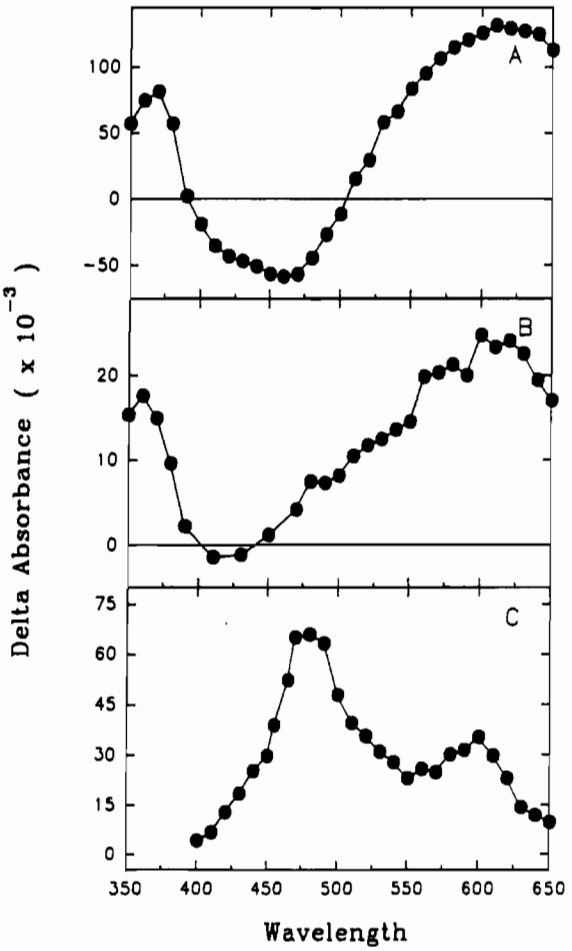

Figure 5. Transient absorption difference spectra at room temperature in CH_3CN for (A) $[Ru^{II}(tpm)(bpy)(MQ^+)]^{3+}$, (B) $[Ru^{II}(tpm)(bpy\text{-}PTZ)(MQ^+)]^{3+}$, and (C) a solution 0.01 mM in $[Ru^{II}(tpm)(bpy)(MQ^+)]^{3+}$ and 11 mM in 10-methylphenothiazine as quencher. The spectra were acquired 25 ns, 50 ns, and 3 μs respectively, following a 420 nm excitation pulse (<4 mJ/pulse).

and 610 nm which correspond to known $\pi \rightarrow \pi^*$ bands in MQ^+, Figure 3. The negative absorption feature (bleach) at 465 nm is consistent with loss of MLCT absorption in the ground state. The intermediate observed following laser flash excitation, Figure 5A, undergoes exponential decay to the ground state with a rate constant $k = (3.3 \pm 0.2) \times 10^6\ s^{-1}$, Figure 6. This value is the same, to within experimental error, as the value determined by time-resolved emission. The same difference spectrum and decay kinetics were observed following excitation at 532 nm. There was no evidence for ligand loss photochemistry even after extended photolysis (2 h, CH_3CN, 0.1 M $[N(n\text{-}C_4H_9)_4]Cl$).

As the temperature was decreased in 4:1 (v:v) ethanol:methanol there was no change in the difference spectrum (Figure 7) but the lifetime of the intermediate increased. There was some evidence in the data for a risetime in the formation of the intermediate below 140 K, but it was irresolvable with our instrumentation (5–10 ns). Upon entering the solvent glass a blue shift in the emission energy occurred (Table III). By 77 K the emission maximum had shifted to 596 nm which coincided with emission from $[Ru(tpm)(bpy)(4\text{-}Etpy)]^{2+}$ at the same temperature, Figure 4A. The decay of the emission at 77 K could be fit to the bi-exponential function in eq 2. In either case >90% of the decay occurred with a lifetime of 3.6 μs, Table III.

$$I(t) = A_1 \exp[-(k_1 t)] + A_2 \exp[-(k_2 t)] \qquad (2)$$

For $[Ru(tpm)(bpy\text{-}PTZ)(py)]^{2+}$ a very weak emission at 664 nm was observed at room temperature which decayed with $\tau <$ 10 ns. No significant transient absorption features were observed from 350 to 700 nm following 460 nm excitation at room temperature. Steady state photolysis in CH_3CN led to rapid photodecomposition as evidenced by changes in the MLCT absorption bands in the visible.

Temperature dependent transient emission and transient absorption data were also acquired on $[Ru(tpm)(bpy\text{-}PTZ)(py)]^{2+}$. The results are summarized in Table IV. Emission decay kinetics were exponential from 253 K to 165 K. Below 165

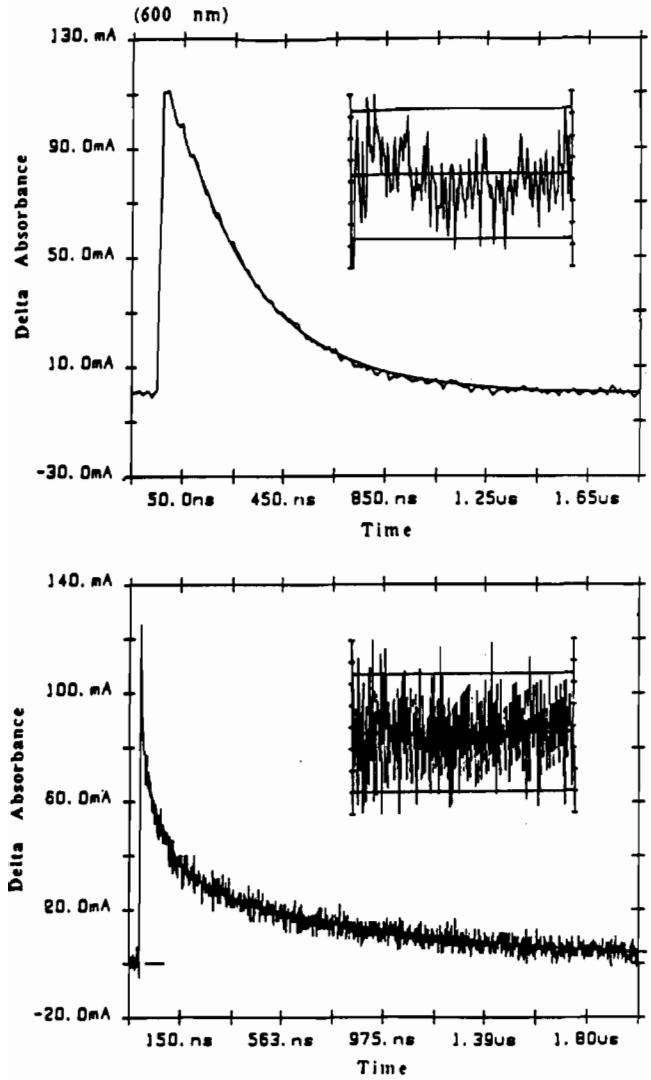

Figure 6. Decay of the transient absorption signal, monitored at 610 nm, for $[Ru^{II}(tpm)(bpy)(MQ^+)]^{3+}$ (top) and $[Ru^{II}(tpm)(bpy\text{-}PTZ)(MQ^+)]^{3+}$ (bottom) in CH_3CN at 295 K following 420 nm excitation (3.2 mJ/pulse). The results of single exponential (top) and biexponential (bottom) fits to the data are shown as overlays on the experimental data. Plots of the residuals of the fits are shown in the insets.

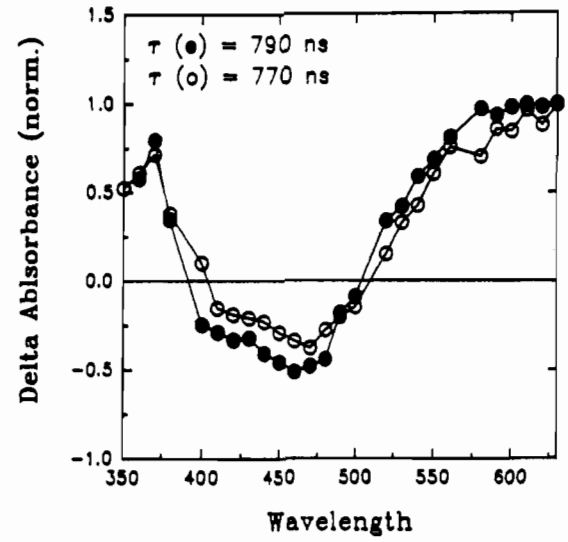

Figure 7. Transient absorption difference spectra for $[Ru^{II}(tpm)(bpy)(MQ)]^{3+}$ (●) and $[Ru^{II}(tpm)(bpy\text{-}PTZ)(MQ)]^{3+}$ (○) in 4:1 ethanol:methanol at 140 K acquired 100 ns following a 420 nm excitation pulse (<4 mJ/pulse). The spectra were normalized to a maximum value of 1 for ΔA at 600 nm. The lifetimes of the transients are shown on the figure.

Table IV. Temperature Dependence of the Lifetime for $[Ru(tpm)(bpy\text{-}PTZ)(py)]^{2+}$ in 4:1 (v:v) Ethanol:Methanol Measured by Emission (τ_{em}) or Absorption (τ_{ab})

temp, K (±3 K)	τ_{em}[a] (ns ± 3%)	τ_{em} or τ_{ab}[b] (ns ± 3%)
77	4370	
145	580 (0.95)/1610 (0.05)	
155	460 (0.94)/1210 (0.06)	
165		880
173		760
178		715
185		670
200		650
216		500
253		80

[a] The excitation wavelength was 460 nm and the emission was monitored at 640 nm. The decay data at 145 and 155 K were fit satisfactorily to the biexponential expression in eq 2. The relative weighting factors for the two components are shown in parentheses. [b] The transient absorption data were acquired following 460 nm excitation and were monitored at 520 nm. The lifetimes were independent of monitoring wavelength at $T > 150$ K and wavelength dependent at $T < 150$ K when the absorption measurements were extended to higher energies.

K they became non-exponential but could be satisfactorily fit to the bi-exponential expression in eq 2. At 77 K in a 4:1 (v:v) ethanol:methanol glass an intense, structured emission was observed. The major features in the transient absorption difference spectrum until 250 K were the expected $\pi \rightarrow \pi^*(bpy^{\bullet-})$ transition at 370 nm and a bleach at ~465 nm. Below 250 K an additional absorption feature appeared at 520 nm and the bleach at 465 nm decreased in intensity. As the temperature was decreased further (<200 K), there was no longer evidence for photochemical decomposition. Below 250 K the decay of the transient absorption features were single exponential, independent of monitoring wavelength (350–700 nm) and the decay constants were the same as for emission, Table IV.

For $[Ru^{II}(tpm)(bpy\text{-}PTZ)(MQ^+)]^{3+}$, which contains both the electron transfer acceptor and donor, there was no appreciable emission at room temperature, Table III. Steady state photolysis in CH_3CN 0.1 M in $[N(n\text{-}C_4H_9)_4]Cl$ led to some decompositions after a period of 1–2 h as evidenced by changes in the UV–visible spectrum. Following laser flash excitation in acetonitrile, absorption features due to reduced MQ^+ appeared at 610 nm and 370 nm, Figure 5B. The intensities of these features were reduced relative to those for $[Ru^{II}(tpm)(bpy)(MQ^+)]^{3+}$ following excitation of solutions of equal absorbance at 420 nm under the same conditions. In addition, a shoulder appeared at ~520 nm (λ_{max} PTZ^+ = 517 nm) and there was no bleach at 465 nm due to the loss of the ground state absorption.

The decay of the transient absorption features for $[Ru^{II}(tpm)(bpy\text{-}PTZ)(MQ^+)]^{3+}$ were non-exponential and wavelength dependent. In CH_3CN at 295 K the decay kinetics could be fit satisfactorily by eq 2 with $k_1 = (1.3 \pm 0.1) \times 10^6\ s^{-1}$, $A_1 = 0.55$, $k_2 = (1.62 \pm 0.05) \times 10^7\ s^{-1}$, and $A_2 = 0.45$ at 370 nm, Table III and Figure 6B. As the temperature was decreased, the emission intensity and lifetimes increased in 4:1 (v:v) ethanol:methanol. The decay of the transient absorption signals was dominated by a component (>90%) having $k = (6.7 \pm 0.3) \times 10^6$, $(5.0 \pm 0.1) \times 10^6$, and $(1.3 \pm 0.1) \times 10^6\ s^{-1}$ at 200, 173, and 140 K respectively when monitored at 600 nm.

Significant changes occurred in the transient absorption difference spectrum below 200 K. In Figure 7 is shown the difference spectrum for $[Ru^{II}(tpm)(bpy\text{-}PTZ)(MQ^+)]^{3+}$ acquired 100 ns after 420 nm excitation at 140 K. It is nearly superimposable with that for $[Ru^{II}(tpm)(bpy)(MQ^+)]^{3+}$ under the same conditions. Upon entering the solvent glass (~130 K) the transient absorption bands for $MQ^{\bullet}$ at 610 and 370 nm decreased. In the rigid glass at 77 K an intense emission was observed at 588 nm, Figure 4B, and its decay kinetics were similar to that for $[Ru^{II}(tpm)(bpy)(MQ^+)]^{3+}$. The decay kinetics were biexpo-

nential (eq 2) with a dominant (>90%), long-lived component ($k = 2.3 \times 10^5\ s^{-1}$), Table III.

Intermolecular, reductive quenching of $[Ru^{II}(tpm)(bpy)(MQ^+)]^{3+}$ by 10-methylphenothiazine (10-MePTZ) in acetonitrile

$$[Ru^{III}(tpm)(bpy)(MQ^{\bullet})]^{3+*} + \text{10-MePTZ} \rightarrow [Ru^{II}(tpm)(bpy)(MQ^{\bullet})]^{2+} + \text{10-MePTZ}^+ \quad (3)$$

was studied by transient absorption measurements. A characteristic difference spectrum obtained in the presence of 11 mM 10-MePTZ is shown in Figure 5C. The difference spectrum is dominated by intense absorption features at 480 and 595 nm similar to the spectra obtained upon one-electron reduction of the complex, Figure 3. There is also evidence for a shoulder at ~520 nm which is an absorption maximum for 10-MePTZ$^+$, Figure 2. It was not possible to extend the measurements below 400 nm because of light absorption by the high concentration of 10-MePTZ.

Quantum Yields. The transient absorption difference spectrum obtained following reductive quenching of $[Ru^{II}(tpm)(bpy)(MQ^+)]^{3+}$ by 10-MePTZ (eq 3 and Figure 5C) provides a model for the difference spectrum that would be expected to appear following laser flash photolysis of $[Ru^{II}(tpm)(bpy\text{-}PTZ)(MQ^+)]^{3+}$ if the redox-separated state, $[Ru^{II}(tpm)(bpy\text{-}PTZ^+)(MQ^{\bullet})]^{3+}$, were formed. The difference spectrum obtained (Figure 5B) is different in two significant aspects: (1) By comparing Figures 5A and 5B, which were obtained under identical conditions, it is apparent that the absorption change in the MQ$^{\bullet}$ region above 600 nm is diminished considerably. (2) By comparing Figures 5B and 5C, the ratio of the absorption change at 450–500 nm to that at ~600 nm ($\pi \rightarrow \pi^*(MQ^{\bullet})$) is greatly diminished.

In order to quantify the first point, transient absorption experiments were conducted in parallel on separate samples containing $[Ru^{II}(tpm)(bpy)(MQ^+)]^{3+}$ and $[Ru^{II}(tpm)(bpy\text{-}PTZ)(MQ^+)]^{3+}$ in acetonitrile which had identical ground state absorbances ($A = 0.25$) at the excitation wavelength (420 nm). Based on relative intensities at 640 nm, where only MQ$^{\bullet}$ absorbs appreciably, a quantum yield of 0.49 (±0.10) was obtained for the appearance of MQ$^{\bullet}$ in solutions containing $[Ru^{II}(tpm)(bpy\text{-}PTZ)(MQ^+)]^{3+}$ relative to $[Ru^{II}(tpm)(bpy)(MQ^+)]^{3+}$. These values were calculated by extrapolating the kinetic decay plots back to $t = 0$ in order to minimize differences in excited state decay.[21-23] For the triad the yield measurement was for –MQ$^{\bullet}$ distributed between two states; $[Ru^{II}(tpm)(bpy\text{-}PTZ^+)(MQ^{\bullet})]^{3+}$ and $[Ru^{III}(tpm)(bpy\text{-}PTZ)(MQ^{\bullet})]^{3+}$, see below.

The ratio of –PTZ$^+$ to –MQ$^{\bullet}$ following excitation of $[Ru^{II}(tpm)(bpy\text{-}PTZ)(MQ^+)]^{3+}$ was estimated by comparing the transient absorption difference spectrum, Figure 5B, with the spectrum obtained following quenching of $[Ru^{II}(tpm)(bpy)(MQ^+)]^{3+}$ by 10-MePTZ, Figure 5C. The absorbances of the solutions were the same at the excitation wavelength (420 nm) and, at the concentrations of 10-MePTZ used (11 mM), the extent of bimolecular quenching was >95%. The difference spectrum for $[Ru^{II}(tpm)(bpy\text{-}PTZ)(MQ^+)]^{3+}$ was acquired 50 ns after the laser flash and for the bimolecular reaction 3 μs after the flash. At 3 μs, quenching was complete but significant back electron transfer between $[Ru^{II}(tpm)(bpy)(MQ^{\bullet})]^{2+}$ and 10-MePTZ$^+$ had not occurred.

The bimolecular quenching reaction gives –PTZ$^+$ (as 10-MePTZ$^+$) and –MQ$^{\bullet}$ in equal amounts, eq 3. Its difference spectrum provides a good measure of the relative spectral features expected following excitation of $[Ru^{II}(tpm)(bpy\text{-}PTZ)(MQ^+)]^{3+}$ if –PTZ$^+$ and –MQ$^{\bullet}$ were formed in equal amounts. The absorptivity above 600 ns is dominated by $\pi \rightarrow \pi^*(MQ^{\bullet})$ and at 450–500 nm by $\pi \rightarrow \pi^*(PTZ^{\bullet+})$ and $d\pi \rightarrow \pi^*(MQ^{\bullet})$ or $d\pi \rightarrow \pi^*(bpy)$. The transient absorption data are consistent with a distribution between $[Ru^{II}(tpm)(bpy\text{-}PTZ^+)(MQ^{\bullet})]^{3+}$ and $[Ru^{III}(tpm)(bpy\text{-}PTZ)(MQ^{\bullet})]^{3+}$. The distribution between the two states was estimated from the transient absorption data on the two solutions by comparing the absorption changes at 510 nm to those at >600 nm. At ~510 nm the ground state and the excited state, $[Ru^{III}(tpm)(bpy\text{-}PTZ)(MQ^{\bullet})]^{3+*}$, are equally absorbing, as shown by the transient absorption spectrum obtained for $[Ru^{III}(tpm)(bpy)(MQ^{\bullet})]^{3+}$ in Figure 5a, and the only contribution to the absorptivity increase is from the redox separated state $Ru^{II}(tpm)(bpy\text{-}PTZ^+)(MQ^{\bullet})]^{3+}$. For bimolecular quenching, $\{\Delta OD(510\ nm)/\Delta OD(640\ nm)\} = 3.3$. For $Ru^{II}(tpm)(bpy\text{-}PTZ)(MQ^+)]^{3+}$ the ratio was 0.67. From the ratio of the two, 0.20, the fraction of $Ru^{II}(tpm)(bpy\text{-}PTZ^+)(MQ^{\bullet})]^{3+}$ in the solution 50 ns after laser flash excitation was 0.20.

Discussion

Redox Properties. For $[Ru(tpm)(dmb)(X)]^{n+}$ (X = Cl$^-$, n = 1; X = H_2O, py, n = 2) reversible $Ru^{III/II}$ oxidations and $bpy^{0/-}$-based reductions appear in cyclic voltammograms.[7b] With bpy-PTZ as a ligand an additional wave appears for the bpy-PTZ$^{+/0}$ couple at $E_{1/2} = +0.80 \pm 0.01$ V. The potentials for these couples are unaffected by coordination, in agreement with previous results for related complexes[9b] and consistent with insignificant electronic coupling between bpy and PTZ through the methylene link.

In $[Ru^{II}(tpm)(bpy)(MQ^+)]^{3+}$ and $[Ru^{II}(tpm)(bpy\text{-}PTZ)(MQ^+)]^{3+}$ three, well-separated, one-electron reductions appear. The sites of reduction cited in Table I can be inferred based on comparisons with electrochemical data for MQ$^+$ and the model complexes.[24-26]

The $E_{1/2}$ values for the $Ru^{III/II}$ and $bpy^{0/-}$ couples are substantially influenced by the nature of the sixth ligand. Exchange of Cl$^-$ for MQ$^+$ leads to an increase in $E_{1/2}(Ru^{III/II})$ of 0.55 V and in $E_{1/2}(bpy^{0/-})$ of ~0.25 V. These variations arise, in part, from electronic effects and changes in the σ donor, π donor/acceptor abilities of Cl$^-$, H_2O, py or MQ$^+$. Increased $d\pi$–π^* interaction in the series stabilizes the metal $d\pi$ orbitals increasing $E_{1/2}$ values for oxidation of Ru^{II} to Ru^{III}. The effects at π^*(bpy) are indirect and transmitted to the bpy ligand by decreased $d\pi$–π^*(bpy) mixing which increases $E_{1/2}(bpy^{0/-})$, but to a lesser degree.

Spectroscopic Properties. The electronic spectra consist of a series of convoluted, ligand-centered (LC) $\pi \rightarrow \pi^*$ and MLCT $d\pi(Ru) \rightarrow \pi^*$ bands based on the different aromatic heterocyclic ligands. For $[Ru^{II}(tpm)(bpy)(MQ^+)]^{3+}$ and $[Ru^{II}(tpm)(bpy\text{-}PTZ)(MQ^+)]^{3+}$, the $d\pi \rightarrow \pi^*$(bpy) and $d\pi \rightarrow \pi^*(MQ^+)$ bands are convoluted and their energies can not be estimated directly from

(21) (a) Carmichael, I.; Helman, W. P.; Hug, G. L. *J. Phys. Chem. Ref. Data* **1977**, *73*, 1319. (b) Carmichael, I.; Hug, G. L. *J. Phys. Chem. Ref. Data* **1986**, *15(1)*, 1. (c) Bensasson, R.; Land, E. J. *Photochemical and Photobiological Rev.*; Smith, K. C., Ed.; Plenum: New York, 1978; Vol. 3, p 163.

(22) Jones, W. E., Jr. Ph.D. Dissertation, The University of North Carolina, 1991.

(23) It can be shown that, for a two-level system, the effect of excited state decay on the excited state concentration produced during the laser pulse is a function of the decay rate constant, k_i, and the duration of the laser pulse, Γ, treated as a square wave excitation, as described by the equation

$$\frac{X_i(0)}{X_i(\Gamma)} = \left[\frac{k_i\Gamma}{(1 - e^{-k_i\Gamma})}\right]$$

In this equation $X_i(0)$ is the amount of excited state produced in the absence of excited state decay and $X_i(\Gamma)$ is the amount of excited state produced when excited state decay is taken into account. With the ~40 ns lifetime for $[Ru(tpm)(bpy\text{-}PTZ)(MQ)]^{3+}$ and the ~8 ns duration of the laser pulse, there was a loss of ~10% of the excited state produced during the laser pulse. This effect was taken into account in calculating the relative formation yields. For a derivation of this equation see ref 18 or: Carmichael, I.; Hug, G. L. *J. Phys. Chem.* **1985**, *89*, 4036.

(24) Osa, T.; Kuwana, T. *J. Electroanal. Chem. Interfacial Electrochem.* **1969**, *22*, 389.

(25) Chen, P.; Curry, M.; Meyer, T. J. *Inorg. Chem.* **1989**, *28*, 2271.

(26) Vlcek, A. A. *Coord. Chem. Rev.* **1982**, *43*, 39.

Scheme I

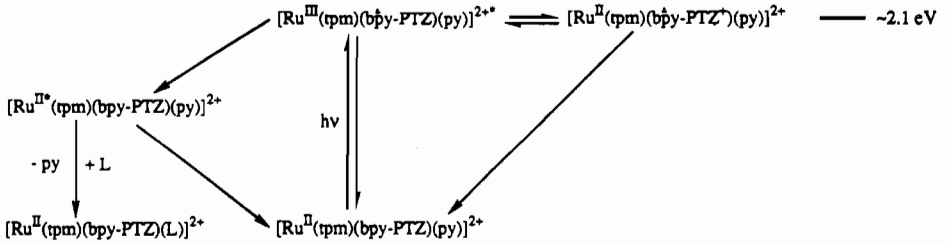

the spectra. For the tpm (and related) complexes a correlation exists between the energy of the lowest energy, intense $d\pi \rightarrow \pi^*$(bpy) MLCT absorption bands and the difference between the redox potentials for the $Ru^{III/II}$ and $bpy^{0/-}$ couples ($\Delta E_{1/2}$).[7,12,27-29] From this correlation and $\Delta E_{1/2}$ for $[Ru^{II}(tpm)(bpy\text{-}PTZ)(MQ^+)]^{3+}$ and $[Ru^{II}(tpm)(bpy)MQ^+]^{3+}$, $d\pi \rightarrow \pi^*$(bpy) is expected at ~21 600 cm^{-1}. It occurs at 21 500 cm^{-1} in $[Ru(tpm)(bpy)(py)]^{2+}$. From the difference spectra in Figure 1, $d\pi \rightarrow \pi^*(MQ^+)$ is at ~21 300 cm^{-1} in $[Ru^{II}(tpm)(bpy)(MQ^+)]^{3+}$ and $[Ru^{II}(tpm)(bpy\text{-}PTZ)(MQ^+)]^{3+}$.

In the spectra of the one-electron reduced forms of the tpm complexes containing $-MQ^+$, $\pi \rightarrow \pi^*(MQ^\bullet)$ bands appear at 360 nm and 595 nm (Figure 3). The ratio of their intensities and energies are comparable to those for 4,4′-bpyH$^\bullet$ (380 and 570 nm) generated by pulse radiolysis of 4,4′-bpy in aqueous solution.[30] An intense, narrow ($\Delta\bar{\nu}_{1/2} \sim 1/2$ that for $d\pi \rightarrow \pi^*(MQ^+)$) also appears at 480 nm which can not be assigned to an intraligand transition. An analogous band appears in the spectrum of the two-electron reduced form of *cis*-$[Ru(bpy)_2(MQ^+)_2]^{4+}$.[31] These bands may arise from $d\pi \rightarrow \pi^*$(bpy) or $d\pi \rightarrow \pi^*(MQ^\bullet)$ transitions and their assignment is currently under investigation.[32]

Excited State Energies. In order to understand the photophysical and photochemical properties of the chromophore–quencher complexes, it is necessary to make estimates for the energies of the various states that are reached after photolysis. They include "excited states", e.g. $[Ru^{III}(tpm)(bpy)(MQ^\bullet)]^{3+*}$ and redox-separated states, e.g., $[Ru^{II}(tpm)(bpy\text{-}PTZ^+)(MQ^\bullet)]^{3+}$. The energies of the excited states can be estimated by spectroscopic measurements and the redox-separated states by electrochemical measurements.

For the $Ru^{III}(dmb^\bullet)$-based excited state in $[Ru(tpm)(dmb)(py)]^{2+}$ (dmb is 4,4′-dimethyl-2,2′-bipyridine) in 4:1 (v:v) ethanol–methanol at room temperature, $\Delta G°_{es} \sim 2.05$ eV.[7b,33] This value provides an estimate for the $Ru^{III}(bpy^{\bullet-})$ excited state energies in $[Ru(tpm)(bpy\text{-}PTZ)(py)]^{2+}$ and $[Ru^{II}(tpm)(bpy\text{-}PTZ)(MQ^+)]^{3+}$. The energy of the redox-separated state, $[Ru^{II}(tpm)(bpy^{\bullet-}\text{-}PTZ^+)(py)]^{2+}$, can be estimated to be ~2.1 eV from the difference in $E_{1/2}$ values for the $-PTZ^{+/0}$ and $bpy^{\bullet-}$-PTZ couples by including a work term correction.[34]

From the electrochemical data in Table I, $-MQ^+$ is a better electron acceptor than bpy or bpy-PTZ by ~0.57 eV from which $\Delta G° \sim 1.5$ eV for the $-MQ^+$-based states in $[Ru^{II}(tpm)(bpy\text{-}PTZ)(MQ^+)]^{3+}$ and $[Ru^{II}(tpm)(bpy)(MQ^+)]^{3+}$. This value is very close to the energy of the emission maximum (795 nm, 1.56 eV) for $[Ru^{II}(tpm)(bpy)(MQ^+)]^{3+}$. Since $E_{em} = \Delta G° - \lambda - \lambda_\theta$ (λ is the reorganizational energy and λ_θ is the contribution to the reorganizational energy from changes in ring–ring rotations at MQ^+, see below). This should be a lower limit for $\Delta G°$. For the redox-separated state, $[Ru^{II}(tpm)(bpy\text{-}PTZ^+)(MQ^\bullet)]^{3+}$, $\Delta G° \sim$ 1.5 eV from the difference in $E_{1/2}$ values for the $-PTZ^{+/0}$ and $-MQ^{+/0}$ couples including the work term correction.

In earlier studies it was found that the dihedral angle between the pyridyl rings of MQ^+ in $[Re^I(bpy)(CO)_3(MQ^+)]^{2+}$ is $\theta = 47°$ in the ground state and it was assumed that $\theta \sim 0$ in the MQ^+-based MLCT excited state, $[Re^{II}(bpy)(CO)_3(MQ^\bullet)]^{2+*}$.[25,37,38] The extent of coplanarity is dictated by a balance between electronic delocalization (enhanced by ring coplanarity) and repulsion between the H-atoms at the 3,3′ positions of the ring. The same changes in relative ring orientation presumably exists in the ground and MQ^+-based MLCT excited state in $[Ru^{III}(tpm)(bpy\text{-}PTZ)(MQ^+)]^{3+}$ and $[Ru^{III}(tpm)(bpy)(MQ^+)]^{3+}$. The change in the dihedral angle between the ground and excited states introduces a contribution to the absorption and emission energies in addition to $\Delta G°$ and the inner- and outer-sphere reorganizational energies.[25,38] This complication must be taken into account when calculating the excited state energies for the MQ^+-based MLCT states from their absorption and emission energies. The value taken for the redox-separated state is that estimated from the electrochemical data.

The energies of the various states are summarized in Schemes I–III in CH_3CN, 0.1 M $[N(n\text{-}C_4H_9)_4](PF_6)$ except for the $Ru^{III}(bpy^{\bullet-})$ and $Ru^{III}(bpy^{\bullet-}\text{-}PTZ)$ excited states which are in 4:1 ethanol–methanol.

Intramolecular Electron Transfer. $[Ru(tpm)(bpy\text{-}PTZ)(py)]^{2+}$. The ligand loss photochemistry and short lifetime for this complex

(27) (a) Sutin, N.; Marcus, R. A. *Comments Inorg. Chem.* **1986**, *6*, 209. (b) Marcus, R. A. *J. Chem. Phys.* **1956**, *24*, 966. (c) Hush, N. S. *Electrochim. Acta* **1968**, *13*, 1005. (d) Marcus, R. A.; Sutin, N. *Biochim. Biophys. Acta* **1985**, *811*, 265. (e) Kober, E.; Hupp, J. T.; Neyhart, G. A.; Meyer, T. J. *J. Phys. Chem.*, in press. (f) Marcus, R. A. *J. Phys. Chem.* **1990**, *94*, 4963.

(28) (a) Lever, A. B. P.; Pickens, S. R.; Minor, P. C.; Licoccia, S.; Ramaswamy, B. S.; Magnell, K. *J. Am. Chem. Soc.* **1981**, *103*, 6800. (b) Curtis, J. C.; Meyer, T. J. *Inorg. Chem.* **1982**, *21*, 1562. (c) Crutchley, R. J.; Lever, A. B. P. *Chem. Phys. Lett.* **1984**, *112*, 567. (d) Juris, A.; Belser, P.; Barigeletti, F.; von Zelewsky, A.; Balzani, V. *Inorg. Chem.* **1986**, *25*, 256.

(29) (a) Meyer, T. J. *Pure Appl. Chem.* **1986**, *58*, 1576 and references therein. (b) Juris, A.; Balzani, V.; Barigelletti, F.; Campagna, S.; Belser, P.; von Zelewsky, A. *Coord. Chem. Rev.* **1988**, *84*, 85 and references therein.

(30) Winkler, J. R.; Netzel, T. L.; Creutz, C.; Sutin, N. *J. Am. Chem. Soc.* **1987**, *109*, 2381.

(31) Sullivan, B. P.; Abruña, H.; Finklea, H. O.; Salmon, D. J.; Nagle, J. K.; Meyer, T. J. Sprintschnik, 11. *Chem. Phys.* **1978**, *58*, 389.

(32) Bignozzi, C. A. Unpublished results.

(33) The value for $\Delta G°_{1\text{-}S}$ is taken as E_{00} obtained by a Franck–Condon analysis of the emission spectral profile.

(34) The energy of the redox-separated state was calculated by $\Delta G° = -\Delta E_{1/2} - w_r$ where

$$w_r = -\frac{e^2}{D_s d(1 + \beta d\mu^{1/2})}$$

The work term includes the coulombic energy of interaction between the charges at (bpy$^\bullet$) and $-PTZ^+$ in the redox-separated state assuming them to be spherical.[10a,35] The quantities D_s and μ are the static dielectric constant and ionic strength of the medium, e the unit electronic charge, d the separation distance between the ions, and $\beta = (8\text{-}\pi N_A e^2/1000 D_s k_B T)^{1/2}$. By using 6 ● 1 Å for d,[36] the magnitude of the work term varies from 0.06 at $\mu = 0$ to 0.07 at $\mu = 0.1$ which gives $\Delta G° \sim 2.1$ eV.

(35) (a) Newton, M. D.; Sutin, N. *Annu. Rev. Phys. Chem.* **1984**, *35*, 437. (b) Meyer, T. J. *Proc. Inorg. Chem.* **1983**, *30*, 389.

(36) This estimate was made by using Chem 3D and bond distances available from crystal structures for a related tpm complex (Llobet, A.; Hodgson, D. J.; Meyer, T. J. *Inorg. Chem.* **1990**, *29*, 3760), as well as for the $-MQ^+$ [25] and $-PTZ$ [39] ligands.

(37) (a) Stephens, F. S.; Vagg, R. S. *Inorg. Chim. Acta* **1982**, *42*, 139. (b) Bukowska-Strzyzewska, M.; Tosik, A. *Acta Crystallogr., Sect. B* **1982**, *B38*, 265, 950. (c) Kubel, F.; Strohle, J. *Z. Naturforsch., B: Anorg. Chem. Org. Chem.* **1982**, *B37*, 272. (d) Julve, M.; Verdaguer, M.; Faus, J.; Tiniti, F.; Moratal, J.; Monge, A.; Gutierrez-Puebla, E. *Inorg. Chem.* **1987**, *26*, 3520.

(38) Chen, P.; Westmoreland, T. D.; Meyer, T. J. Manuscript in preparation.

Scheme II

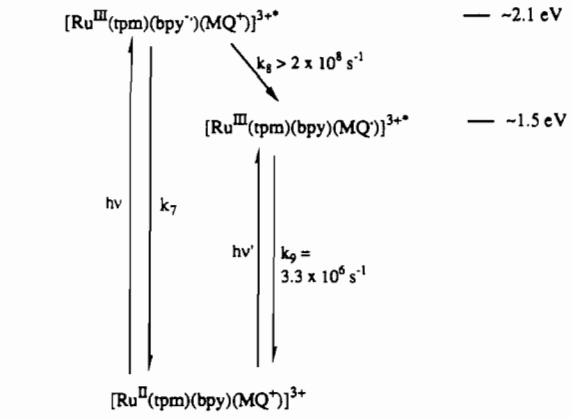

in CH_3CN at room temperature are reminiscent of [Ru(tpm)-(bpy)(4-Etpy)]$^{2+}$.[7b] Decay of the MLCT excited state(s) is presumably dominated by population and subsequent decay or ligand loss from a low-lying ligand field (dd) state or states, eqs 4 and 5. There is no evidence for the redox-separated state,

$$\xrightarrow{h\nu} [Ru^{III}(tpm)(bpy^{\bullet-}\text{-}PTZ)(py)]^{2+*} \rightarrow [Ru^{II*}(tpm)(bpy\text{-}PTZ)(py)]^{2+} \quad (4)$$
$$(d\pi)^5(\pi^*)^1 \qquad (d\pi)^5(d\sigma^*)^1$$

$$[Ru^{II*}(tpm)(bpy\text{-}PTZ)(py)]^{2+} \xrightarrow{-py,\ +L} [Ru^{II}(tpm)(bpy\text{-}PTZ)(py)]^{2+},\ [Ru^{II}(tpm)(bpy\text{-}PTZ)(L)]^{2+} \quad (5)$$

[Ru^{II}(tpm)(bpy$^{\bullet-}$-PTZ$^+$)(py)]$^{2+}$ formed by intramolecular electron transfer, Scheme I. It may play a role, but never buildup because of equilibrium with the MLCT state and decay via the ligand field state, Scheme I.

The MLCT→dd transition in [Ru(tpm)(bpy)(4-Etpy)]$^{2+}$ has a significant activation energy (3200 cm^{-1} in 4:1 (v:v) EtOH/MeOH) and the dd state plays a lessened role in excited state decay as the temperature is decreased. This appears to be the case for [Ru^{II}(tpm)(bpy-PTZ)(py)]$^{2+}$ as well. As the temperature is decreased emission appears from [Ru^{III}(tpm)-(bpy$^{\bullet-}$-PTZ)(py)]$^{2+*}$ which can be time-resolved, τ = 80 ns at 253 K, Table IV. Evidence for intramolecular electron transfer and the equilibrium in Scheme I is obtained in the transient absorption spectrum with the appearance of the characteristic absorption feature for –PTZ$^+$ at λ_{max} = 517 nm. The transient absorption and emission decays occur with the same rate constant and independent of monitoring wavelength. This observation is consistent with a rapid equilibrium between the excited and redox-separated states on the time scale of the excited state decay. By 200 K the decay lifetime had increased to 650 ns, suggesting only a minor contribution from the ligand field state.

At temperatures below 155 K emission decay became non-exponential and an apparent risetime appeared in the transient absorption traces at 517 nm that was convoluted with the laser pulse. The decay data could be fit satisfactorily to biexponential kinetics, Table IV. Apparently, at this temperature the time scales for intramolecular electron transfer and excited state decay are comparable and coupling between their kinetics causes the nonexponentiality.

By 77 K emission intensities and lifetimes are nearly those of [Ru(tpm)(bpy)(4-Etpy)]$^{2+}$, Table III, and there is no evidence for intramolecular electron transfer. Quenching of intramolecular electron transfer in rigid media has been observed in other chromophore–quencher complexes. The effect has been attributed to a decrease in the driving force arising from the frozen orientations of the solvent dipoles in the glass.[4a,10a,35,39]

[Ru(tpm)(bpy)(MQ$^+$)]$^{3+}$. The excited state properties of this complex in CH_3CN are consistent with rapid (τ < 5 ns) formation of [Ru^{III}(tpm)(bpy)(MQ$^\bullet$)]$^{3+*}$ following Ru^{II}→bpy, Ru^{II}→MQ$^+$ excitation at 420, 460, or 532 nm. This conclusion is based on the appearance of the red-shifted, weak emission at ~795 nm, the absorption features for MQ$^\bullet$ at 370 and 610 nm in the transient absorbance difference spectrum (Figure 5A) and the bleach at 465 nm for the loss of Ru^{II}→bpy and Ru^{II}→MQ$^+$ bands in the ground state. Either Ru^{II}→bpy or Ru^{II}→MQ$^+$ excitation leads to the same excited state showing that bpy$^{\bullet-}$→MQ$^+$ electron transfer is rapid, eq 6, k(25°, CH_3CN) > 2 × 10^8 s^{-1}.

$$\xrightarrow{h\nu} [Ru^{III}(tpm)(bpy^{\bullet-})(MQ^+)]^{3+*} \rightarrow [Ru^{III}(tpm)(bpy)(MQ^\bullet)]^{3+*} \quad (6)$$

The weak, red-shifted emission is from the state [Ru^{III}(tpm)-(bpy)(MQ$^\bullet$)]$^{3+*}$, as shown by the coincidence of its decay kinetics with those for loss of MQ$^\bullet$ by transient absorption. Similar, red-shifted MQ$^\bullet$ or 4,4′-bpy$^{\bullet-}$-based emissions have been reported for [Re(bpy)(CO)$_3$(MQ$^+$)]$^{2+}$ [10a] and [(4,4′-(CH$_3$)$_2$-bpy)-(CO)$_3$Re^I(4,4′-bpy)Re^I(CO)$_3$(4,4′-(CH$_3$)$_2$-bpy)]$^{2+}$.[40]

This complex is photostable, suggesting that intramolecular electron transfer is more facile than MLCT→dd state interconversion ($k_5 \ll k_6$ in eq 7), and that the MQ$^\bullet$-based state is too

$$\xrightarrow{h\nu} [Ru^{III}(tpm)(bpy^{\bullet-})(MQ^+)]^{3+*} \xrightarrow[k_6]{k_5} [Ru^{II*}(tpm)(bpy)(MQ^+)]^{3+*} \quad (7)$$
$$(d\pi)^5(\pi^*_{bpy})^1 \qquad (d\pi)^5(d\sigma^*)^1$$
$$[Ru^{III}(tpm)(bpy)(MQ^\bullet)]^{3+*}$$
$$(d\pi)^5(\pi^*_{MQ^\bullet})^1$$

low in energy to populate the ligand field state significantly during its lifetime. The rate constants are k_6 (CH_3CN, 298 K) > 2 × 10^8 s^{-1} from this work and k_5 (4:1 EtOH/MeOH, 298 K) = 3 × 10^6 s^{-1} in [Ru(tpm)(bpy)(4-Etpy)]$^{2+}$.[7b] The effect of the ligand field state on lifetimes is illustrated by τ < 14 ns for [Ru^{III}(tpm)(bpy$^{\bullet-}$)(4-Etpy)]$^{2+*}$ and τ = 300 ns for [Ru^{III}(tpm)-(bpy)(MQ$^\bullet$)]$^{3+*}$ even though the excited state energy for the latter is lower by ~1900 cm^{-1}. The photophysical events that occur following MLCT excitation of [Ru(tpm)(bpy)(MQ$^+$)]$^{3+}$ in CH_3CN at room temperature are summarized in Scheme II.

The characteristic absorption features of [Ru^{III}(tpm)(bpy)-(MQ$^\bullet$)]$^{3+*}$ in the transient absorption spectrum were retained in 4:1 (v:v) EtOH:MeOH until the glass-to-fluid transition was reached at ~120 K, Figure 7. The lifetime increased from 300 ns at 298 K to 790 ns at 140 K.

Below the glass-to-fluid transition, emission is dominated by Ru^{II}(bpy$^{\bullet-}$). There is evidence for a lower energy Ru^{III}(MQ$^\bullet$) emission, and emission decays were non-exponential at 77 K. Similar observations have been made and rationalized for [Re(bpy)(CO)$_3$(MQ$^+$)]$^{2+}$.[10a,22,38,39]

[Ru^{II}(tpm)(bpy-PTZ)(MQ$^+$)]$^{3+}$. A CHEM 3D molecular structure of the donor–chromophore–acceptor triad, is shown in Figure 8 in a conformation that minimizes the distance between –PTZ and –MQ$^+$ (6 Å). The complex is essentially non-emitting in CH_3CN at room temperature. There was evidence for ligand-loss photochemistry, but it was inefficient.

Transient absorption measurements reveal the presence of an intermediate or intermediates formed during the laser pulse, Figure 5B. Characteristic absorption features for –MQ$^\bullet$ (370 and 610 nm) and a broad absorption feature in the visible for –PTZ$^+$ (517 nm) appear in the spectra. The bleach at 465 nm, which appears following excitation of [Ru^{II}(tpm)(bpy-PTZ)-

(39) Jones, W. E., Jr.; Chen, P.; Meyer, T. J. *J. Am. Chem. Soc.* **1992**, *114*, 387.
(40) (a) Tapolsky, G.; Duesing, R.; Meyer, T. J. *Inorg. Chem.* **1990**, *29*, 2285. (b) Duesing, R.; Tapolsky, G.; Meyer, T. J. *J. Am. Chem. Soc.* **1990**, *112*, 5359.

Scheme III

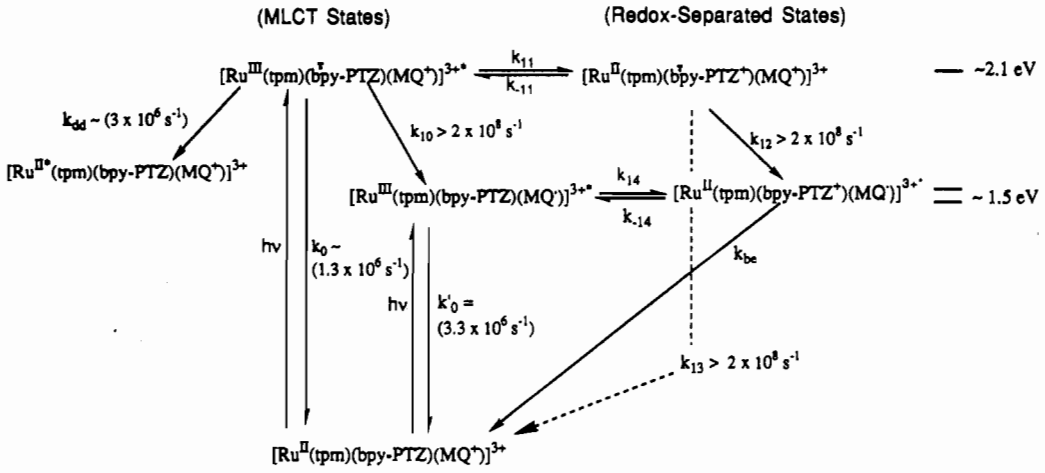

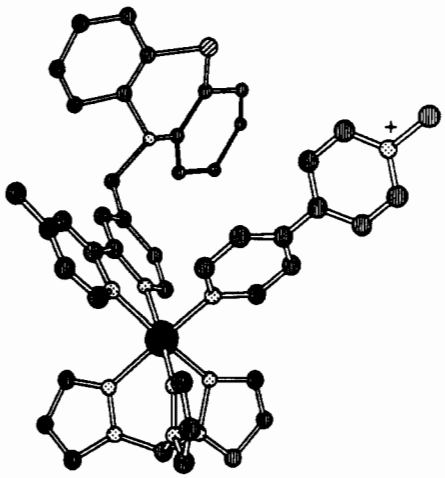

Figure 8. Three-dimensional structure of $[Ru^{II}(tpm)(bpy\text{-}PTZ)(MQ^+)]^{3+}$, calculated by using Chem 3D.[43]

$(MQ^+)]^{3+}$ due to the loss of $Ru^{II}\rightarrow$bpy, MQ^+ absorption, was not observed. The decay of the transient absorption signal was non-exponential and dependent on monitoring wavelength. Absorption vs time traces could be fit to biexponential kinetics, an example is shown in Figure 6.

From these observations it can be inferred that $Ru^{II}\rightarrow$bpy-PTZ, MQ^+ excitation leads to two states $[Ru^{III}(tpm)(bpy\text{-}PTZ)(MQ^{\bullet})]^{3+*}$, and by the absence of the bleach in the visible, to $[Ru^{II}(tpm)(bpy\text{-}PTZ^+)(MQ^{\bullet})]^{3+}$. From the comparison between $\Delta\mathcal{A}(510)/\Delta\mathcal{A}(640)$ for $[Ru^{II}(tpm)(bpy\text{-}PTZ)(MQ^+)]^{3+}$ with that for the bimolecular quenching of $[Ru^{III}(tpm)(bpy)(MQ^{\bullet})]^{3+*}$ by 10-MePTZ, Figure 5C, the fraction of $-PTZ^+$ formed relative to $-MQ^{\bullet}$ was ~0.20, 50 ns after laser flash. The fact that both appear is consistent with the estimate for the energy difference between states of ~0 eV.

From the non-exponential decay kinetics for the mixture of states, it can be inferred that interconversion between them (k_{14},k_{-14}, in Scheme III) occurs on a time scale comparable to their decays (k_0' and k_{be}). Similar observations have been made for related Ru–bpy complexes containing bpy-PTZ.[41] This means that the distribution between states is time dependent and they are not in equilibrium. In principle, a kinetic analysis of the data is possible since the set of differential equations describing a reversible kinetic coupling between two states which decay to a single state has been solved.[3c,18] The analysis predicts bi-exponential decay kinetics as observed. However, the absence of emission and the overlap of the transient absorption signals for the two states preclude its quantitative application of the analysis to our data and we were unable to evaluate the rate constant for back electron transfer (k_{be} in Scheme III).

There are three electron transfer pathways which could lead to the redox-separated state following $Ru^{II}\rightarrow$bpy-PTZ, MQ^+ excitation, eqs 8–10. In the first, eq 8, $Ru^{II}\rightarrow MQ^+$ excitation

$$\xrightarrow{h\nu} [Ru^{III}(tpm)(bpy\text{-}PTZ)(MQ^{\bullet})]^{3+*} \rightarrow [Ru^{II}(tpm)(bpy\text{-}PTZ^+)(MQ^{\bullet})]^{3+} \quad (8)$$

$$\xrightarrow{h\nu} [Ru^{III}(tpm)(bpy^{\bullet-}\text{-}PTZ)(MQ^+)]^{3+*} \rightarrow [Ru^{III}(tpm)(bpy\text{-}PTZ)(MQ^{\bullet})]^{3+} \rightarrow [Ru^{II}(tpm)(bpy\text{-}PTZ^+)(MQ^{\bullet})]^{3+} \quad (9)$$

$$\xrightarrow{h\nu} [Ru^{III}(tpm)(bpy^{\bullet-}\text{-}PTZ)(MQ^+)]^{3+*} \rightarrow [Ru^{II}(tpm)(bpy^{\bullet-}\text{-}PTZ^+)(MQ^+)]^{3+} \rightarrow [Ru^{II}(tpm)(bpy\text{-}PTZ^+)(MQ^{\bullet})]^{3+} \quad (10)$$

is followed by $PTZ\rightarrow Ru^{III}$ electron transfer. In the second, eq 9, $Ru^{II}\rightarrow$bpy-PTZ excitation is followed by sequential $bpy^{\bullet-}\text{-}PTZ\rightarrow MQ^+$, $PTZ\rightarrow Ru^{III}$ electron transfer. In the third, eq 10, the sequence of electron transfer events following excitation is reversed.

There are additional pathways to the redox-separated state involving intramolecular energy transfer via the $Ru^{III}(bpy^{\bullet-}\text{-}PTZ)$ excited state, eq 11, or by direct excitation, eq 12. We presume that these pathways do not play an important role because of weak electronic coupling between the states involved.

$$\xrightarrow{h\nu} [Ru^{III}(tpm)(bpy^{\bullet-}\text{-}PTZ)(MQ^+)]^{3+*} \rightarrow [Ru^{II}(tpm)(bpy\text{-}PTZ^+)(MQ^{\bullet})]^{3+} \quad (11)$$

$$[Ru^{II}(tpm)(bpy\text{-}PTZ)(MQ^+)]^{3+} \xrightarrow{h\nu} [Ru^{II}(tpm)(bpy\text{-}PTZ^+)(MQ^{\bullet})]^{3+} \quad (12)$$

The combined quantum yield for the appearance of $[Ru^{III}(tpm)(bpy\text{-}PTZ)(MQ^{\bullet})]^{3+*}$ and the redox-separated state (0.49 ± 0.10) is lower by ~$^1/_2$ than for $[Ru^{III}(tpm)(bpy)(MQ^{\bullet})]^{3+*}$. A competition between $bpy^{\bullet-}\rightarrow MQ^+$ and $bpy^{\bullet-}\rightarrow -PTZ^+$ electron transfer to return to the ground state, (k_{13} in Scheme III) could explain the decrease.

The various processes that occur are summarized in Scheme III. In this scheme the rate constants for the MLCT→dd (k_{dd}) and decay of $Ru^{III}(bpy^{\bullet-}\text{-}PTZ)$ (k_0) are values estimated for

(41) Danielson, E. Unpublished results.

$[Ru(tpm)(dmb)(py)]^{2+}$ in 4:1 EtOH–MeOH at 295 K.[7b] Decay of $Ru^{III}(MQ^{\bullet})$ (k_0') is the experimental value for $[Ru^{III}(tpm)(bpy)(MQ^{\bullet})]^{3+*}$ in CH_3CN at 298 K. The redox-separated states $[Ru^{II}(tpm)(bpy^{\bullet-}\text{-}PTZ^{+})(MQ^{+})]^{3+}$ and $[Ru^{II}(tpm)(bpy\text{-}PTZ^{+})(MQ^{\bullet})]^{3+}$ are not shown as being accessible by direct excitation because of the low absorptivities expected for the absorption bands for $bpy\text{-}PTZ \rightarrow bpy^{\bullet-}\text{-}PTZ^{+}$ and $bpy\text{-}PTZ \rightarrow MQ^{+}$ either through the $-CH_2-$ bridge or through space. The absence of significant ligand-loss photochemistry is consistent with rapid $bpy^{\bullet-}\text{-}PTZ \rightarrow MQ^{+}$ electron transfer ($k_{10} > 2 \times 10^8\ s^{-1}$) compared to MLCT→dd ($k_{dd} \sim 3 \times 10^6\ s^{-1}$).

The relative ordering of the $Ru^{III}(MQ^{\bullet})$ and redox-separated states in Scheme III is only an estimate based on the electrochemical measurements and the ordering could be inverted.

The transient absorption features for $d\pi \rightarrow \pi^*(MQ^{\bullet})$ (480 nm) and $\pi \rightarrow \pi^*(PTZ^{+})$ (520 nm) disappeared as the temperature was decreased in 4:1 (v:v) ethanol–methanol. By 140 K there was no evidence for the redox-separated state. Difference spectra and decay kinetics for $[Ru^{II}(tpm)(bpy\text{-}PTZ)(MQ^{+})]^{3+}$ (770 ns) and $[Ru^{II}(tpm)(bpy)(MQ^{+})]^{3+}$ (790 ns) were both single exponential and the same to within experimental error, Figure 7. At temperatures below the glass to fluid transition in 4:1 (v:v) ethanol–methanol at 130–140 K, the emission properties were essentially the same as those of $[Ru(tpm)(bpy)(py)]^{2+}$. From these observations it can be inferred that quenching of $Ru^{III}(bpy^{\bullet-})$ by electron transfer to $-MQ^{+}$ or from $-PTZ$ no longer plays a role at low temperature or in the glass.

The relative ordering of states, $[Ru^{III}(tpm)(bpy\text{-}PTZ)(MQ^{\bullet})]^{3+*} \sim [Ru^{II}(tpm)(bpy\text{-}PTZ^{+})(MQ^{\bullet})]^{3+}$, was not anticipated in the design of the complex, but is easily rationalized, Scheme IV. The oxidizing strength of $[Ru(bpy)_3]^{3+}$ is greater by ~0.5 eV than that of $[Ru^{III}(bpy)_2(bpy^{-})]^{2+*}$. The decrease in the excited state potential is due to the bound bpy radical anion which stabilizes Ru^{III}.[42] The potentials of the excited state and $PTZ^{+/0}$ couples are comparable. Normally, oxidation of the excited state would be followed by spontaneous $-PTZ \rightarrow Ru^{III}$ electron transfer. However, in $[Ru^{III}(tpm)(bpy^{\bullet-}\text{-}PTZ)(MQ^{+})]^{3+*}$ intramolecular oxidation occurs to a second acceptor ligand (MQ^{+}) which is also strongly coupled electronically to Ru^{III} and stabilizes the higher oxidation state. Intramolecular electron transfer converts one MLCT excited state into another, Schemes II and III. The $Ru^{III}(MQ^{\bullet})$ excited state is lower in energy than $Ru^{III}(bpy^{\bullet-})$ but the decrease is in the enhanced electron acceptor ability of MQ^{+} compared to bpy. The $Ru^{III/II}$ potentials are nearly the same in the two excited states.

Scheme IV

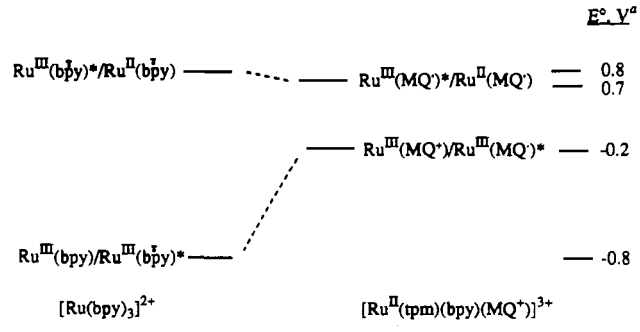

[a] in CH_3CN ($\mu = 0.1$) vs. SSCE.

Acknowledgments are made to the National Science Foundation under Grant No. CHE-9022493 (T.J.M.) and NATO-CNR (for a Senior Fellowship in 1989 to C.A.B.) for financial support.

(42) Lumpkin, R.; Murtaza, Z.; Worl, L.; Kober, E. M.; Meyer, T. J. In preparation.
(43) Jovanic, M. V.; Biehl, E. R.; Rosenstein, R. D.; Chu, S. C. *J. Heterocycl. Chem.* **1984**, *21*, 661.